# Displacement-based design procedure of grouted anchoring systems for the seismic upgrade of heritage buildings

Authors: Victor Melatti [*a)], Dina D'Ayala [a)]

[a)] Department of Civil, Environmental and Geomatic Engineering, University College London, WC1E 6BT, UK

*Corresponding author. Tel.: +44 (0) 7542457437

E-mail address: ucesvme@ucl.ac.uk (V. Melatti), d.dayala@ucl.ac.uk (D. D'Ayala)

## 1 *Abstract*

A displacement-based design procedure is proposed to control the out-of-plane motion of masonry walls during seismic events by means of a Grouted Anchoring System (GAS) and a Dissipative Grouted Anchoring Systems (D-GAS). Combining the non-linear static capacity of walls in three different configurations (unstrengthened, strengthened with GAS or D-GAS) with the inelastic demand spectra gives the expected performance of the system, which is then compared to a set of damage thresholds corresponding to the progression from linear to nonlinear behaviour of the system. The design method is validated comparing the expected performance with the evolution of the wall's rocking motion obtained by means of time-history analysis for a seismic acceleration adapted to the design spectrum used in the static analysis. The results highlight that the D-GAS provides the optimal design solution as it controls the amplitude and acceleration of the rocking motion while dissipating the seismic energy through friction. This allows for a reduced number of required anchors, thus a less invasive of the intervention, which is beneficial especially for applications to historical building with aesthetic value.

***Keywords**: Dissipative anchoring system, steel grouted anchors, friction device, rocking of masonry walls, displacement-based design procedures.*

## 1. Introduction

Analysis of the damage suffered by monumental masonry buildings exposed to seismic events [1–3] highlights that their load bearing elements often separate into macroelements [4,5], which in turn are characterized by a mostly independent structural behaviour with respect to the rest of the building [6,7]. Churches, for instance, often experience such disconnections and partial failures, due to the low tensile strength of the masonry, their large structural spans (wide halls, high unrestrained façades, etc) and their intrinsic architectonic complexity (presence of bell-towers, vaults, apses and structural systems with different stiffness). Poor-quality connections between orthogonal structural walls greatly affect the dynamic performance of heritage masonry structures causing the relative detachment of masonry walls and ultimately the out-of-plane failure of the most vulnerable macroelements, while other portions of the building survive the shaking, as shown in Fig. 1.

a) b)

Fig. 1 Out-of-plane damages caused by earthquakes to monumental buildings: a) Christchurch (NZ) 2011, b) Norcia (IT) 2016.

For the past two centuries this structural weakness has been mitigated by introducing metal cross-ties placed along the masonry walls at the level of the horizontal elements and at corner connection between orthogonal walls. For this retrofitting solution, external anchor plates bolted to the ties redistribute the tension load in the ties to a portion of masonry, restoring the box-like behaviour and restraining the out-of-plane movement of these walls. In historic masonry buildings (HMB), the presence of elements of value such as frescos and decorations, encourages the use of injected anchors placed within the thickness of the walls. The installation of injection anchors is advantageous in comparison to tie rods and anchor plates since it minimizes the aesthetic impact on the structure and facilitates the intervention on façade walls requiring access from only one side of the wall. The performance of anchors injected in masonry substrates are typically investigated by means of experimental pull-out tests [8–14]. These tests represent an effective way to reproduce – statically – the forces exerted on the grouted anchors and to determine the corresponding failure modes.

The attained maximum load capacity informs the design procedures which typically follow a Force-Based (FB) approach. According to Code's recommendations [15,16], the design of the anchoring system is performed by simply considering the ultimate overturning equilibrium of the macro element modelled as rigid blocks, given the peak ground acceleration ($a_g$), corresponding to a specific site and return period for the life safety performance level. In the equilibrium equation, the contribution of the anchoring system to the stability of the wall under lateral load is proportional to the maximum load capacity obtained from pull-out tests, via large safety factors.

Using this simple method, the number and dimensions of anchors per metre height of the wall, needed to prevent the wall from overturning due to the seismic action, can be determined.

Nonetheless, this approach presents several shortcomings. The use of the peak ground acceleration to derive the seismic demand comes from the assumption that unreinforced masonry (URM) possesses very limited ductility, so that the strengthened system is designed to maintain the system in its elastic range, assuming that any lateral deformation is transient, considering this the only safe configuration [4]. Therefore, the peak ground acceleration, namely the acceleration corresponding to infinitely stiff foundation solidly connected to a perfectly rigid upper structure, is considered the governing parameter to compute the seismic demand and the anchors are dimensioned to remain in their elastic phase for the expected seismic acceleration. For acceleration demands corresponding to high magnitude earthquakes, this may lead to over-dimensioned ties and anchoring plates, and unfeasible designs, especially for historic buildings where minimum intervention criteria may limit the number and sizing of the intervention [10]. Moreover, the increased local stiffness at the anchor's location might lead to high-stress concentration in case of seismic events and consequently to severe damage to the valuable parent material in which the cross-ties are embedded [17].

Experimental research has shown that seismically-excited unreinforced masonry walls can display out-of-plane (OOP) rocking motion without overturning, which allows the walls to sustain accelerations well in excess of their "quasi-static" capacity [18–20] . By accounting for the post-elastic displacement capacity of a wall, the seismic vulnerability of the macroelements, prone to local damage and collapse mechanisms, can be evaluated also according to different methods within the framework of Displacement-Based (DB) design [21,22]. DB design methods for strengthening systems consider the ductility capacity that the whole structural system can provide to adequately reduce the seismic demand, thus reducing intrusiveness of the strengthening interventions.

Nonetheless, the design of grouted anchors as an aseismic strengthening provision based on a performance-based approach is hampered by the evidence from pull-out tests showing that ductility provided by grouted anchors is frequently limited and highly unpredictable [10]. Therefore, grouted anchors are currently designed to work in the elastic range and their ductility is considered as an additional capacity that the wall can potentially develop during the seismic event [11].

An anchorage system to remedy this pitfall was investigated by [23] who propose the use of a Dissipative Grouted Anchoring System (D-GAS) for grouted anchors, to provide a source of quantifiable and stable ductility. Of the two devices proposed in [23], the friction-based device underwent further development and refinement and two prototypes, named FEPCyl and BraCyl, were manufactured and underwent extensive testing [24]. The revised devices are characterised by two frictional interfaces made of Fluorinated Ethylene Propylene (FEP) and brass that improve the performance under cyclic loading and ensure corrosion protection, and by a cylindrical shape of the internal slider that reduces the intrusiveness for installations in historic structures.

The principle underlying the functioning of this D-GAS is that the device exploits and controls the rocking behaviour that monumental structures often exhibit during earthquakes [25], providing the anchors with ductility and energy dissipation capacity and preventing the brittle failure of grouted anchors. The stable behaviour under cyclic loading and the displacement capacity of the dissipative device allows for the use of DB methods to design the seismic strengthening of a historic structure.

The aim of this study is to provide a design procedure for grouted anchoring systems in historic masonry structures built in seismic areas. This method aims at addressing the technical gap in current regulations [15,16] whereby no clear procedures for the design of these systems are provided, besides qualitative indications.

In the first part of the paper, a literature review of experimental tests performed on steel grouted anchors embedded in masonry is presented to construct a database of parameters required to underpin the proposed design procedure. Specifically, the maximum pull-out load, displacement capacity and failure modes for each experimental campaign are reported and normalised to determine values of generic validity for design purposes.

Drawing on this database, a non-linear model is developed to compute the lateral force capacity of walls in their original configuration and with anchoring systems to control their out-of-plane motion. Currently the design of the anchors can be performed in terms of load capacity, following the FB approach suggested by the Italian code [15]. Herein a displacement capacity approach is proposed, by applying the N2 method procedure proposed in the Eurocode 8 [16]. To achieve this, first a set of threshold displacements corresponding to the progression from linear to nonlinear behaviour of the system, is identified, then the performance point coordinates are computed, and the required ductility compared with the system's available ductility.

Two different configurations are proposed for grouted anchors, without and with a friction base dissipative device, respectively. Non-linear time history analyses are performed to compare the dynamic damaging sequence and failure modes for the wall unstrengthen, with GAS and with D-GAS.

To focus the discussion on the benefits of the GAS and D-GAS to practical engineering applications, the design method is applied to the oratory of San Giuseppe dei Minimi, a church that suffered severe, but repairable out-of-plane triggered damage, during the 2009 seismic events in L'Aquila, Italy [26].

The vulnerability of the front wall to OOP failure is assessed by static and dynamic analysis, revealing that the original structure is in need of seismic strengthening. To this purpose, the grouted anchors provided by Cintec international, industrial partner of this research, and the dissipative device developed by [24] are considered to control the OOP motion of the façade. The analysis is repeated for different design solutions obtained according to the FB approach and the DB method presented in this work.

It is found that the DB method provides a safer design for the traditional anchoring system compared to the FB method: the limited displacement capacity provided by GAS calls for a check in displacements to ensure that the demand is smaller than the capacity or alternatively that the FB design is performed considering the system with no ductility capacity.

The dissipative system represents the optimal design solution, as the inclusion of the dissipative device allows controlling the wall's displacement below the damage thresholds even with a 50% reduction in the number of required anchors. Because the N2 method allows for a reduction of the seismic demand which is directly proportional to the ductility capacity of the system, the adjustable displacement capacity of the device leads to a smaller acceleration demand and therefore less anchors are required to counteract the seismic action. This leads to a less invasive strengthening intervention and reduces the impact on the original aesthetic and structural authenticity of the building.

## 2 Literature review of pull-out tests on anchors embedded in masonry elements

Several experimental pull-out tests of grouted anchors have been performed in the last decades [8–14]. The tests aim at determining a reliable estimate of pull-out force depending on the numerous parameters that can influence the behaviour of grouted anchors, such as type of masonry substrates, anchor's material, surface and length of embedment, grout thickness and strength, presence of stress transversal to the anchors, spacing between anchors, distance between anchors and wall's edge, etc. Due to the uncertainty in the anchor's behaviour, pull-out tests are also carried out in-situ before installation under the same procedures of experimental tests to verify the load bearing capacity of the anchor and substrate. Given the lack of specific design clauses for anchors in masonry, the tests are performed according to the same protocols used for pull-out test of anchors in concrete substrata and of masonry bed-joint reinforcement, such as [27,28], or according to the considerations of existing literature [9,29]. Seven experimental programs performed by different authors on different anchor types are presented. To the author judgment and knowledge, this represents the most comprehensive set of experimental programs performed on metallic grouted anchors to discuss the influence of the abovementioned parameters on the load and ductility capacity. Results of pull-out tests performed on grouted anchors made of Fiber Reinforced Plastic (FRP) are not included in this analysis as the objective is to determine the feasibility of a displacement design approach for grouted stainless-steel ties. Anchoring systems by means of metallic rods have been extensively explored and are already widely applied by professionals in conservation engineering, as they are cost effective and conforming to current conservation recommendations. Therefore, the focus of the study is on this anchor typology.

The experimental results are used to construct the databased presented in Table 1 and to investigate the reliability of the available analytical formulations (presented in section 2.2) to predict the load capacity of the anchors.

### 2.1 Review of pull-out test on anchors embedded in masonry

For grouted anchors installed in masonry substrates, the observed experimental failure modes as classified by [30] are:

- Cone Masonry Detachment failure (CMD), characterized by the detachment of a pseudo-conic portion of masonry around the anchor whose geometry is determined by the typology of masonry fabric, i.e. size of the units and thickness of the mortar joints.
- Bond failure at bar/grout interface, characterized by slippage of the anchor from the surrounding grout (SBG);
- Bond failure at grout/masonry interface, characterized by slippage of the grout sleeve from the masonry (SGM);
- 'Mixed' failure characterized by the joint detachment of a masonry cone or slippage of bricks adjacent to the outer portion of the anchor and the slippage of the grout sleeve from the masonry (MIX).

The notation proposed by [10] is used in this work to designate the anchor's capacity. The use of the term *slip* refers to the point at which the anchors reach their maximum load capacity. The relative motion between the anchor and the masonry, according to the failure mode displayed at the end of each test, is indicated as *elongation* and includes the elastic deformation of the rebar.

The first comprehensive experimental program aimed at filling the lack of code regulations on the load capacity provided by grouted anchors in masonry substrates were carried out by Gigla [8,31,32] . He performed more than 500 pull-out tests over several years on injected anchors embedded in clay bricks [8] and clay brick panels [31]. The author evidenced the positive effect of compressive stresses in the masonry around the anchor, with an increment of pull-out load by almost 40% when the compressive stress increased from 0 to 0.4MPa. Based on the experimental results, analytical formulations were proposed to correlate the bond strength of grouted anchors to the compressive strength of the injected grout. Additional tests were carried out on different types of steel bars (stainless and ordinary steel ribbed bars, threaded rods) with diameter 16 mm and embedded length of 200 mm in monolithic sandstones [32]. Threaded rods provided a more effective bond behaviour with small displacements compared to the ribbed bars, which attained an ultimate load only 10% lower. Ribbed stainless steel bars attained the best performance in terms of both ultimate load and ductility.

Arifovic [9] carried out an extensive experimental program on ribbed steel bars in clay bricks samples to observe the failure modes of grouted anchors and correlate it to their maximum loads capacity. Pull-out tests had highlighted that different failure modes may occur, due to the interaction of different materials (i.e. masonry, injection grout, anchor) and the presence of two interfaces (i.e. masonry-grout and grout-anchor). For each failure mode a set of analytical formulations were obtained by applying the theory of plasticity for anchors in masonry in analogy of the anchorage theory developed for anchors embedded in concrete [33,34] .

In [10] the performance of a grouted anchoring system patented by Cintec International was tested on walls made of Victorian clay bricks. These anchors have a fabric sleeve wrapped around the rebar that expands as grout is injected into it thus moulding into the shape and space within the wall. In this way, the grout flow is controlled, ensuring an even distribution along the embedment length and the expansion within the wall's voids provides additional mechanical bonding. The bars were embedded in two panels by means of cement-based grout and subjected to different average vertical compressive stresses (0.08–0.09 MPa and 0.7 MPa). When the higher compressive stresses were present, the ultimate load was in average 20% higher and a bond failure at grout-masonry interface occurred. Conversely, in case of lower compressive stresses, a mixed failure was observed. In addition, cyclic tests were performed on samples of T-shaped walls to investigate the seismic performance of grouted anchors and the influence of interaction between walls. A reduced maximum pull-out load was observed in cyclic tests results compared to monotonic pull-out load. This reduction was likely due to the lower compressive strength of the mortar used in the T-shaped wall.

The authors identify three main points on the capacity curve of the grouted anchor: point A corresponds to load and displacement obtained at first damage, point B corresponds to the maximum pull-out force $F_t$ and *slip elongation* $d_s$, while point C refers to ultimate force $F_u$ and *elongation* $d_u$ when a loss of 20% load carrying capacity occurs, i.e. $F_u = F_t * 0.8$ [35]. Beyond point C, the load capacity eventually drops, and the anchor reaches its ultimate capacity, unless further mechanical locking, arising while the anchor slides out of the cavity, allows for a further increase in stiffness.

The authors propose a dimensioning procedure based on the strength capacity of the tested connection and on the assumption that the maximum load capacity of the anchor assembly should be larger than the seismic demand expected for the Ultimate Limit State (ULS), namely for the acceleration calculated for a seismic action with a probability of exceedance of 10% in 50 years [16]. The ductility, computed as the ratio between the displacement at point C and point B, presents a narrow range of values and the average ductility is 1.9 (CoV = 56%) and 2.4 (CoV = 24%) for monotonic and cyclic loading, respectively. Nonetheless, the displacements present a scattered distribution, the average yielding and ultimate displacement are 1.9 mm (CoV = 46%) and 3.7 mm (CoV = 60%) for the monotonic pull-out tests, and 5.3 (CoV = 136%) and 10.9 (CoV = 30%) for cyclic loading (see Fig. 3a). Therefore, full exploitation of the anchors' potential also in terms of displacement capacity is not explored and displacement considerations are discussed only to ensure the compliance with the requirements on interstory drift [15,16].

A set of tests on the same anchor technology tested by [10] were performed by [11] by means of pull-out tests on grouted anchors embedded in masonry limestone walls reproducing a typical masonry typology for a historic masonry building, to explore the influence on the anchor's performance of masonry substrates having weak mechanical properties (significantly smaller compressive strength of masonry compared to [10] as shown in Table 1). The maximum loads of the bars placed at top of the walls showed a capacity approximately 30%, lower than the bars placed at the bottom, thus, confirming the positive effect of higher compressive stresses in the masonry around the bars. In this case, the cyclic behaviour also shows a degradation of strength capacity and stiffness with increasing cycles and an accumulation of residual displacements. A mixed failure characterized by cone masonry detachment and bond failure occurred in all tests. The anchors at the top displayed a larger ductility capacity compared to the ones at the bottom, confirming that the anchors can provide a ductile connection, favourable for seismic performance.

A third extensive experimental program of pull-out tests was carried out by [12] using the same anchoring technology tested by [10]. The bonded length ($l_e = 400$ and 900 mm), the compressive vertical loading in the masonry walls (0.05, 0.1, 0.2MPa), the compressive strength of the grout (49 and 59 MPa for cement-based grouts, 9 MPa for lime-based grout), the strength and layout of mortar joints, and the loading history (monotonic or cyclic) are the parameters investigated.

The results provided by [12] showed little to no influence of the compressive stress on the anchor strength for low values of stress (0.05 or 0.1 MPa), while an increase of about 30% of the ultimate load occurred in case of stress equal to 0.2 MPa, in line with Gigla's results. The CMD failure never occurred confirming that the cone failure is unlikely to happen for "long" anchor, namely anchors with $l_e > 40\sqrt{d_h}$ where $d_h$ is the diameter of the borehole. Conversely a SGM failure mode was frequently observed, in few cases jointly with the slippage of 2–3 adjacent bricks around the outer portion of the anchor (MIX mode). It was observed that the cyclic load history reduced the anchor strength of 20% in comparison with the same specimens tested under monotonic loads.

In [13] the performance of injected anchors was studied, performing pull-out test on different types of masonry, changing the masonry units (clay bricks and vertically perforated units) and the type of mortar. Two series of in situ pull-out tests were carried out on injected anchors embedded in yellow tuff masonry walls. Anchors were embedded for 300 mm by means of cement-based and "pozzolana"-based grout, the latter having a significant lower compressive strength. The experimental results evidenced that a MIX failure was obtained for the cement-based grout, while the pozzolana grout led to lower pull-out loads and SBG failure.

Regarding the rebar materials, different solutions have been explored besides steel bars, such as, Glass Fibre Reinforced Plastic (GFRP) [14], Carbon Fibre Reinforced Plastic bars (CFRP ) [14,36].

In [14], the performance of innovative anchors made of GFRP and CFRP were compared to that of traditional steel ribbed bars. A special surface treatment was also made by wrapping the FRP bars with stainless steel fabrics (SRP) embedded in a putty to increase the bond performance along the injected grout/bar interface. The anchors were embedded in masonry prisms made of yellow tuff blocks. It was found that these anchors display a similar or slightly better performance in terms of pull-out capacity compared to traditional steel anchors, when surface treatments are implemented. The ductility capacity is also similar, with the exception of the GFRP which display a long, stable ductile behaviour but a smaller strength capacity.

Following up on the work reported in [10] in [36] a T-shaped masonry wall was tested to determine the improvement in the connection between orthogonal walls by means of a hollow pultruded carbon tubes (CFRP). The authors concluded that the system can significantly increase the horizontal force applied to the wall compared to an unrestrained

wall, preventing the formation of cracks. Moreover, the tests highlight that effective strengthening solutions can increase the ultimate displacement and thus energy dissipation capacity of the wall.

The review of existing literature on injected anchors herein presented has evidenced the influence of the embedment length on the performance of anchors, in terms of load capacity and type of failure mode. Long anchors mainly fail for a SGM mode and present larger maximum pull-out loads as the anchor grips on a larger portion of masonry. Accordingly, it is found that surface treatment of the anchors and the properties of injection grout positively influence the performance as they increase the mechanical boning between the components of the anchor and the surrounding material. In particular, the comparison of the results obtained using Cintec's anchors [10–12] with the results reported by [8,9] have highlighted that the fabric sleeve contributes to improve the displacement capacity of the grouted anchor. The mechanical locking between the bulges of the sleeve and the masonry cavity increases the range of displacement at sustained peak strength.

On the other hand, it was observed a degradation in load capacity and a larger variability in such displacement capacity under cyclic behaviour, suggesting that at present the extra strength obtained through the grouting cannot be fully exploited in a reliable way.

The use of innovative materials such as FRP can increase the ultimate displacement of the anchor, providing energy dissipation capacity and ductility to the strengthened connection. Nonetheless, few experimental programmes have been performed for this anchoring technology so that conclusive correlation between loading condition, capacity and failure mode can hardly be drawn, and further experimental evidence are needed.

### 2.2 Literature formulas to predict pull-out load of grouted anchors

Depending on the failure mode activated by the pull-out test, several formulations for predicting the maximum pull-out force of injected anchors in masonry elements are available in literature [8,9,34].

For the ***Cone Masonry Detachment (CMD)***, the analytical formulation inferred by Arifovic [9] through experimentally based regression is:

$$F_{max} = 0.96\, h_{cone}^2 \sqrt{f_{c,m}} \tag{1}$$

where, $f_{c,m}$ is the compressive strength of the masonry and $h_{cone}$is the depth of the cone portion of masonry that is contributing to the pull-out force. The CMD is experimentally observed for "short" anchors ($l_e < 40\sqrt{d_h}$), for which the value of $h_{cone}$ can be assumed equal to the embedment length $l_e$.

For the ***Bond Failure at Bar/Grout Interface (SBG),*** the empirical formulation provided by Gigla [8] is :

$$F_{max} = \tau_g\, \pi\, d_b\, l_e \tag{2}$$

where:

$$\tau_g = \Phi_j \left(\frac{f_{c,g}^2}{500}\right) \tag{3}$$

The bond strength, $\tau_g$, mainly depends on the compressive strength of the grout,$f_{c,g}$, and $\Phi_j$ is a reducing factor (set equal to 0.5 or 0.6 [.] [8] for bed or head joints). There are 2 assumed distribution of shear stress for grouted anchors in concrete which are usually applied also to anchors embedded in masonry. One considers a constant distribution of stress along the embedment length, assumed for instance in Eq. (3) and valid for $l_e < 40\sqrt{d_h}$, and a second that assumes a decaying distribution of the shear stresses with the embedded length, which is recommended for $l_e > 40\sqrt{d_h}$ in [37]. According to the latter stress distribution, the maximum pull-out force is computed as:

$$F_{max} = \pi\, \tau_g d_b \left(\frac{\sqrt{d_b}}{\lambda'} \tanh\left(\frac{\lambda'\, l_e}{\sqrt{d_b}}\right)\right) \tag{4}$$

where $d_b$ is the diameter of the bar and $\lambda'$ is an elastic constant defined as:

$$\lambda' = \sqrt{\frac{4G_g}{tE_s}} \tag{5}$$

Where $G_g$ is the shear modulus of the grout, $t$ is the wall's thickness and $E_s$ is the elastic modulus of the bar. For short anchors, Eq. (2) and (4) yield the same values of pull-out force. For long anchors, Eq. (4) should be considered because the linear correlation between embedment length and pull-out force is not supported by experimental evidence for $l_e > 40\sqrt{d_h}$.

For ***Bond Failure at Grout-Masonry Interface (SGM),*** Eq.(6) is proposed by [9]:

$$F_{max} = C_1\, d_b\, l_e \sqrt{f_{c,m}} \tag{6}$$

This formula can be interpreted as a variation of Eq. (2) where the bond strength at the grout-masonry interface is expressed as function of the square root of the masonry compressive strength, as frequently assumed for the bond strength of steel bar-concrete interface [33] and $C_1$ is empirically determined by numerical regression. It should be noted that Eq. (6) was derived by [9] for anchors with small embedment length $l_e < 40\sqrt{d_h}$ for which the hypothesis of uniform stress distribution is valid. Similar to the SBG failure, for anchors of length $l_e > 40\sqrt{d_h}$ the maximum pull-out force can be computed as:

$$F_{max} = C_2\, \pi \sqrt{f_{c,m}}\, d_b \left( \frac{\sqrt{d_b}}{\lambda'} \tanh\left( \frac{\lambda'\, l_e}{\sqrt{d_b}} \right) \right) \tag{7}$$

In Eq. (7), proposed by [38], $C_2 = 1$ is obtained based on experimental pull-out tests performed on adhesive anchors embedded in concrete specimens. Both Eq. (6) and (7) are derived for anchors with borehole's diameter $d_h$ almost identical to the diameter of the bar (see values in Table 1 for [9]), which explains why the $d_b$ is considered despite the fact that the formula addresses the failure at the grout-masonry interface. Nonetheless, for anchor typologies with larger ratio between $d_h$ and $d_b$ such as the Cintec's anchorage, the borehole's diameter should be used to compute the maximum force and different values of $C_1$ and $C_2$ needs defining (see section 2.3).

Finally, for the ***'Mixed' failure mode (MIX)***, the following formulation is proposed [34,39]:

$$F_{max} = C_3\, \pi \sqrt{f_{c,m}}\, d_h \left( \frac{\sqrt{d_h}}{\lambda'} \tanh\left( \frac{\lambda'\, (l_e - h_{cone})}{C_3 \sqrt{d_h}} \right) \right) \tag{8}$$

This failure mode is frequently observed, and the pull-out force should be calculated as the sum of the two contributions previously introduced for cone and grout/masonry failure. Nonetheless as observed both for concrete [37] and masonry [14] substrates, the contribution offered by the cone portion is small compared to the bonding contribution and therefore it is neglected in Eq. (8). Consequently, the embedment length is reduced by $h_{cone}$, which can be assumed as the minimum permissible effective embedment length, i.e. the greater between 51mm and 4 times the diameter of the anchor according to [39,40]. A value of $C_3 = 34.7$ was obtained by numerical regression. Alternatively, Eq. (9) proposed by Arifovic [9] can be adopted:

$$F_{max} = \left[ C_4 \sqrt{f_{c,m}}\, (l_e - h_{cone}) d_b + C_5 \sqrt{f_i} (l_u + d_b) d_b \right] \sqrt{\frac{d_b}{l_e}} \tag{9}$$

Eq. (9) is made of two terms, where the first one is similar to the one proposed by the same authors for SGM failure (see Eq. (6)) with the embedment length reduced by $h_{cone}$, and, thus, is related to the bond stress contribution. The second term depends on the compressive strength of the mortar joint/ brick interface, $f_i$, and on the length of the masonry unit, $l_u$. Lacking specific indication, $f_i$ can be assumed equal to the minimum value between the compressive strength of the mortar of the joints and of the masonry unit. In [9] the values of $C_4$ and $C_5$ are 3.93 and 37.44 respectively. As discussed for Eq. (6) and (7) the pull-out force provided by Eq. (9) should be computed considering the borehole's diameter if $d_h$ is significantly larger than $d_b$.

The numerical factors in Eq. (6), (7), (8) and (9) are introduced so that the analytical prediction could comply with the experimental values of pull-out force for each failure mode. Therefore, the validity of these empirical formulations is highly dependent on the experimental conditions of the performed tests. Many authors [10,11,13,41] found that these formulations can lead to large overestimation or to too conservative predictions of maximum pull-out load, if the grouted anchors and the masonry wall present significantly different geometry and mechanical properties.

In light of these considerations and of the results of seven experimental programmes presented in the next section, alternative values for the numerical factors in Eq. (6), (7), (8) and (9) are presented to obtain a better correspondence between the experimental values and the analytical predictions.

### 2.3 Correlations of experimental and analytical formulations

A compendium of data obtained by experimental tests and a comparison of the strength capacity of different anchorage system is presented in [14]. In the present study that database is extended by considering the displacement and ductility capacity of these tests. These are presented in Table 1. The *slip elongation* $d_s$, *ultimate elongation* $d_u$ are defined as already defined in section 2.2. using the approach introduced by [10]. The ductility factor $\mu$ is computed as the ratio between $d_u$ and $d_s$. Pull-out tests where the embedment length is shorter than $40\sqrt{d_h}$ are not included in this analysis, as short anchors are not a feasible option to connect orthogonal walls and are therefore outside the scope of this work. For two experimental activities, the vertical confinement pressure $\sigma_c$ was not available (n.a.).

Table 1. Experimental database of grouted anchors embedded in masonry

| Authors | Test type | $l_e$ [mm] | $d_h$ [mm] | $d_b$ [mm] | fc,g [MPa] | fc,m [MPa] | Anchor no. | $\sigma_c$ [MPa] | $F_{max\ (M)}$ [KN] | $d_y$ [mm] | $d_u$ [mm] | μ [-] | Failure type |
|---|---|---|---|---|---|---|---|---|---|---|---|---|---|
| Paganoni & D'Ayala, 2014 | MONOTONIC | 350 | 80 | 16 | 50 | 6.7 | a | 0.7 | 60 | 2.8 | 3.8 | 1.4 | SGM |
| | | | | | | | b | | 64 | 1.8 | 2.1 | 1.2 | SGM |
| | | | | | | | c | | 54 | 1.0 | 1.6 | 1.5 | SGM |
| | | | | | | | d | 0.08 | 58 | 3.3 | 6.0 | 1.8 | SGM |
| | | | | | | | e | 0.09 | 40 | 1.6 | 6.6 | 4.1 | SGM |
| | | | | | | | f | | 52 | 1.1 | 1.8 | 1.6 | SGM |
| | CYCLIC | 220 | | | | 3.1 | 1T | 0.08 | 10.9 | 0.8 | 2.5 | 3.2 | MIX |
| | | | | | | | 2T | | 17.8 | 5.1 | 10.0 | 2.0 | MIX |
| | | | | | | | 3T | | 21.9 | 10.0 | 20.1 | 2.0 | MIX |
| Gigla,2004 | CYCLIC | 172 | 30 | 10 | 18.2 | 20 | a | 0.4 | 51 | 0.5 | - | - | SBG |
| | | | | | | | b | 0.3 | 42.5 | 0.5 | - | - | SBG |
| | | | | | | | c | 0 | 38 | 0.2 | 0.5 | 2.4 | SBG |
| Moreira et al., 2014 | CYCLIC | 350 | 50 | 20 | 51.5 | 1.7 | a_t | 0.2 | 55.85 | 2.5 | 6.8 | 2.7 | CMD |
| | | | | 16 | | | b_t | | 53.6 | - | - | - | CMD |
| | | | | 16 | | | c_t | | 52.45 | 2.7 | 9.5 | 3.5 | CMD |
| | | | | 20 | | | a_b | | 40.6 | 0.7 | 12.1 | 17.3 | MIX |
| | | | | 16 | | | b_b | | 37.5 | 0.9 | 6.7 | 7.4 | MIX |
| | MONOTONIC | 350 | | 20 | | | a_b | 0.2 | 38.4 | 3.1 | 16.8 | 5.4 | MIX |
| | | | | 16 | | | b_b | | 37.15 | 1.3 | 7.7 | 5.9 | MIX |
| Arifovic &Nielsen, 2006 | MONOTONIC | 185 | 14 | 12 | 75 | 21.1 | A.2.1 | n.a.d | 35.8 | 1.2 | 2.0 | 1.7 | CMD |
| | | | | | | | A.2.2 | | 41.7 | 1.5 | 1.8 | 1.2 | CMD |
| | | | | | | | A.2.3 | | 34 | 1.4 | 1.6 | 1.1 | MIX |
| | | 230 | 18 | 16 | | | A.2.4 | | 63.1 | 2.3 | 2.8 | 1.2 | SGM |
| | | | | | | | A.2.5 | | 36.8 | 1.4 | 3.0 | 2.1 | MIX |
| | | | | | | | A.2.6 | | 33.7 | 1.4 | 3.0 | 2.1 | MIX |
| | | 185 | 14 | 12 | | | A.2.19 | | 28.3 | 1.5 | 2.5 | 1.7 | MIX |
| | | | | | | | A.2.20 | | 36.3 | 1.6 | 2.5 | 1.6 | SGM |
| | | | | | | | A.2.21 | | 35.9 | 1.5 | 2.0 | 1.3 | MIX |
| | | 230 | 18 | 16 | | | A.2.22 | | 40.5 | 1.6 | 2.0 | 1.3 | MIX |
| | | | | | | | A.2.23 | | 73.4 | 2.3 | 3.0 | 1.3 | MIX |
| | | | | | | | A.2.24 | | 55.7 | 2.0 | 3.0 | 1.5 | MIX |

Table 1 Experimental database of grouted anchors embedded in masonry. [Part 2]

| Authors | Test type | $l_e$ [mm] | $d_h$ [mm] | $d_b$ [mm] | fc,g [MPa] | fc,m [MPa] | Anchor no. | $\sigma_c$ [MPa] | $F_{max\ (M)}$ [KN] | $d_y$ [mm] | $d_u$ [mm] | μ [-] | Failure type |
|---|---|---|---|---|---|---|---|---|---|---|---|---|---|
| Silveri et al., 2016 | MONOTONIC | 400 | 20 | 60 | 50 | 18 | Wall 1 | 0.05 | 40.78 | 1.0 | 2.3 | 2.3 | SGM |
| | | | | | | | | | 77.04 | 2.0 | 3.6 | 1.8 | SGM |
| | | | | | | | | | 53.88 | 1.0 | 1.9 | 1.9 | SGM |
| | | | 60 | 20 | 50 | | Wall 2 | 0.1 | 37.58 | 0.5 | 2.9 | 5.9 | SGM |
| | | | | | | | | | 85.15 | 2.0 | 6.4 | 3.2 | SGM |
| | | | | | | | | | 42.93 | 0.2 | 3.0 | 15.0 | SGM |
| | | | | | | | Wall 2 | 0.1 | 55.08 | 1.0 | 2.1 | 2.1 | SGM |
| | | | | | | | | | 62.3 | 3.0 | 5.9 | 2.0 | SGM |
| | | | | | | | | | 50.69 | 1.0 | 2.2 | 2.2 | SGM |
| | | | | | | | Wall 3 | 0.2 | 54.8 | 1.1 | 2.4 | 2.1 | SBG |
| | | | | | | | | | 90.01 | 2.0 | 3.8 | 1.9 | SBG |
| | | | | | | | | | 77 | 1.0 | 2.1 | 2.1 | SBG |
| | CYCLIC | | | | | | Wall 6 | 0.06 | 35.01 | 1.4 | - | - | SGM |
| | | | | | | | | | 45.75 | 1.5 | - | - | SGM |
| | | | | | | | | | 37.27 | 3.7 | - | - | SGM |
| | | | | | | | Wall 7 | 0.06 | 32.5 | 0.9 | - | - | SGM |
| | | | | | | | | | 44.55 | 2.0 | - | - | SGM |
| | | | | | | | | | 36.6 | 1.5 | 4.6 | 3.0 | SGM |
| | | | | | | | Wall 8 (lime mortar) | 0.06 | 27.22 | 3.8 | - | - | MIX |
| | | | | | | | | | 45.9 | 0.8 | - | - | SGM |
| | | | | | | | | | 29.3 | 1.3 | - | - | SGM |
| | MONOTONIC | 900 | | | | | Wall 9 | 0.06 | 126.27 | 2.5 | - | - | MIX |
| | | | | | | | Wall 10 | | 159.39 | 3.2 | - | - | MIX |
| | | | | | | | Wall 11 | | 183.7 | 4.1 | - | - | MIX |
| | | | | | | | Wall 12 | | 110.82 | 5.2 | - | - | MIX |
| | CYCLIC | | | | | | Wall 13 | 0.06 | 118.2 | 2.1 | - | - | MIX |
| | | | | | | | Wall 14 | | 138.1 | 6.5 | - | - | MIX |
| | | | | | | | Wall 15 | | 98.13 | 5.3 | - | - | MIX |
| | | | | | | | Wall 16 | | 131.29 | 4.1 | - | - | MIX |
| | | | | | | | Wall 17 | | 57.96 | 0.6 | - | - | MIX |
| | | | | | | | Wall 18 | | 100.29 | 13.5 | - | - | MIX |
| Ceroni et al. 2016 | MONOTONIC | 300 | 50 | 20 | 43.4 | 2 | SC_1 | n.a.d | 57 | 6.0 | 10 | 1.7 | MIX |
| | | | | | | | SC_2 | | 65 | 7.0 | 9 | 1.3 | MIX |
| | | | | | | | SC_3 | | 49.7 | 5.0 | 10 | 2.0 | MIX |
| | | | | | 12.6 | | SP_1 | | 50.4 | 3.0 | 7 | 2.3 | SBG |
| | | | | | | | SP_2 | | 47 | 8.0 | 11 | 1.4 | SBG |
| | | | | | | | SP_3 | | 45.6 | 3.0 | 5 | 1.7 | SBG |
| Ceroni et al. 2020 | MONOTONIC | 250 | 25 | 10 | 7.65 | 6.05 | MS10_1 | 0.4 | 32.7 | 2.0 | 3.5 | 1.8 | MIX |
| | | | | | | | MS10_2 | 0.4 | 25.5 | 2.0 | 3.5 | 1.8 | MIX |
| | | | | | | | MS10_3 | 0.4 | 31 | 2.0 | 7 | 3.5 | MIX |

Fig. 2 shows the results of the anchors tested in each experimental programme for monotonic and cyclic loading. The relative displacement of the anchor with respect to the wall is normalized to the value of embedment length $l_e$ to obtain the longitudinal slip strain for the maximum and ultimate load. Even though only long anchors are reported, and the analysis is restricted to grouted anchors made of steel, the results' comparison between testing programmes is not straightforward because each test has been performed under different conditions. Nonetheless, a few observations are possible.

In terms of strain, for cyclic loading, a fairly good agreement is found between the data reported by Paganoni [10], Moreira [11] and Silveri [12]. The average yielding and ultimate strain are about 0.005 (CoV = 15%) and 0.01 (CoV = 47%), which correspond to an average ductility factor of 2. In [11], larger values of ultimate longitudinal strain are obtained, possibly because two anchors, placed close to each other, were pulled simultaneously, causing a mixed failure mode that combines the sliding between the grout/masonry interface and the detachment of a masonry cone. The larger values of pull-out load obtained by [12] are expected due to longer embedment length $l_e$ and large vertical load $\sigma_c$. Gigla [8], Arifovic [9]and Ceroni [13,14] who investigated traditional injected anchors obtained a smaller value of average ductility factor, namely μ = 1.7 (CoV = 32%).

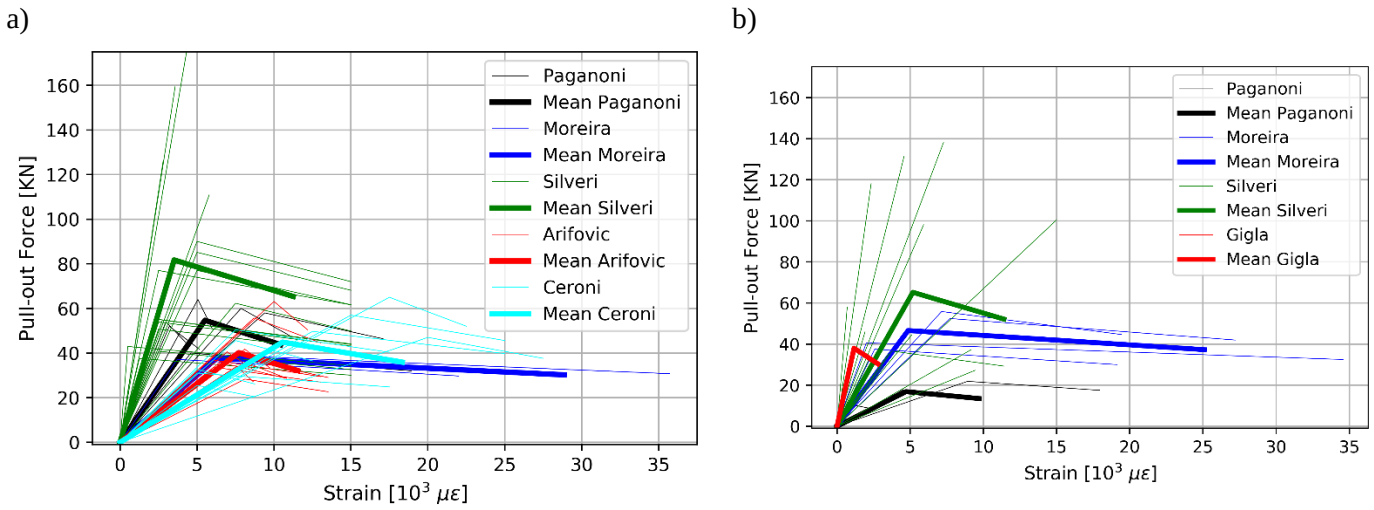


Fig. 2. Capacity curves of grouted anchor under a) monotonic loading and b) cyclic loading

In Fig. 3, the maximum pull-out loads found experimentally are compared to the analytical values predicted by Eq. 6-9 depending on the observed failure mode. The accuracy of the analytical formulas to predict the experimental results is measured considering the mean and Coefficient of variation, CoV, for each failure mode. The mean value of each dataset is indicated by a larger marker to better visualize if a formulation is conservative (the mean value is above the horizontal dotted line) or overestimates the anchor's capacity (the mean value is below the horizontal dotted line).

Of 71 pull-out tests analysed, 33 anchors failed for slippage of the grouted cylinder (SGM failure), 27 for the combined slippage at the grout/masonry interface and cone detachment (MIX failure) and 6 for slippage at the bar/grout failure (SBG failure), 5 for cone failure (CMD failure). For the SBG failure, both Eqs. (2) and (4) underestimate the anchor's capacity by one order of magnitude. Nonetheless, the number of pull-out tests that displayed this failure mode is considered too small to derive conclusions of statistical relevance and the SBG failure is not included in Fig. 3.

For the SGM and MIX failure, alternative values of the numerical constants are presented in Table 2 to compensate for using the borehole's diameter in place of the bar diameter in Eq. (6), (7) and (9) and to obtain a better correlation between analytical and experimental results in (7) and (8) as they were obtained for concrete specimens. For sake of comparison, the experimental-to-analytical ratios are reported in Fig. 3 both for the numerical constants defined by [9,39] in Fig. 3a and for those obtained in this work (Fig. 3b).

Table 2. Values of numerical constants for analytical formulation to predict the maximum pull-out force

| | $C_1$ | $C_2$ | $C_3$ | $C_4$ | $C_5$ |
|---|---|---|---|---|---|
| Arifovic [9] | 3.79 | - | - | 3.93 | 37.44 |
| Cook [39] | - | 1 | 34.7 | - | - |
| This study | 0.5 | 0.28 | 3 | 2 | 30 |

For the SGM failure, the analytical formulations provide opposite results: Fig. 3a shows that Eq. (7) overestimates the pull-out force, while Eq. (8) gives a conservative prediction and in both cases the variance is above 50%. On the other hand, Fig. 3b shows better agreement between experimental and analytical values and values of variance below 50%, proving that $d_h$, and thus alternative constants, should be used in the formulations for SGM. Moreover, Fig. 3b highlights what suggested by [42]: a uniform model can be used to predict the anchor's pull-out load in case of weak substrates even for values of $l_e > 40\sqrt{d_h}$.

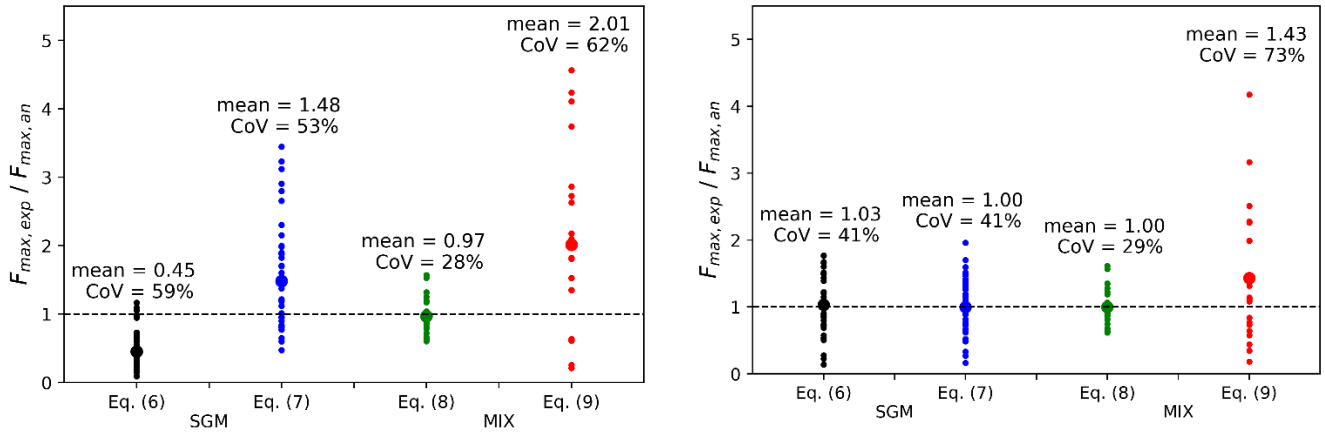


Fig. 3 Comparison between experimental and analytical values of pull-out force depending on the observed failure mode. The analytical values are computed according to the numerical constants defined a) by [9,39], b) by the authors of this study

For the MIX failure, the elastic model expressed by Eq. (8) gives the best results both in terms of average ratio and scatter with a variance below 30%. Similar to the SGM, Eq. (9) benefits from using $d_h$ in place of $d_b$ as better agreement is achieved between experimental and analytical results, even if the scatter remains largely above 50%.

In conclusion, the review of pull-out tests performed on grouted anchors with long embedment length highlights the expected failure modes to occur when the maximum pull-out force is attained. The experimental tests show that either the bond failure at the grout/masonry interface (SGM), or the mixed failure (MIX) with the detachment of a masonry cone and the slippage of the grout sleeve, are the more common failure modes. The other two failure modes are rarely observed: the simple cone failure (CMD) is relevant to anchors with short embedment length, and thus not applicable to anchors connecting orthogonal walls. The failure at grout/bar interface (SGB) is observed in few cases as the bonding strength developed between the rebar and the grout is usually larger than the one developed between the grout and the masonry. Moreover, some anchoring technologies, such as the Cintec anchors have a locking system at the end of the sleeve that prevent any relative slippage between the two inner elements.

Comparing the analytical formulations with the experimental values of pull-out force allows for a critical assessment of the models describing the stress distribution along the anchors. It is found that assuming a decaying distribution of shear stress gives the best results for the MIX mode, while both the uniform and the decaying stress distribution well describe the ultimate load for anchors failing according to the SGM mode. In the last analysis, the smaller value of force provided by Eq. (6)-(8) and reduced by appropriate design safety factors can be adopted as design load for the anchor. The definition of such design factors is outside the scope of this work and should reflect the level of knowledge the user can achieve for instance of the mechanical properties of the masonry substrate by means of destructive/non-destructive tests.

For design applications in real cases, the dimensioning of the strengthening system should be performed favouring the yielding of the rebar over the shear debonding of the anchor as the latter is a ductile failure mode. Nonetheless, the yielding of the bar is rarely observed in experimental and in-situ pull-out tests, possibly because the composite action of high-strength grout and bar provides a larger tensile capacity compared to the bar on its own. Therefore, the design of “long” grouted anchors as anti-seismic system should be performed ensuring that the strength and elongation capacity attained either for the SGM or MIX failure mode are the governing parameter of the design. This consideration further highlights the need to introduce a dissipative component, such as the one proposed in this work, able to improve the behaviour of grouted anchors and avoid their brittle failure.

## 3 Structural assessment of walls strengthened by grouted anchors

The review of pull-out tests highlights that grouted anchoring systems (GAS) display a ductile behaviour after the maximum load is reached. Nonetheless, it is also clear that under cyclic load the strength capacity progressively decreases, hindering the applicability of grouted anchors to strengthen the connections of masonry structures built in seismic prone areas. For such applications, anti-seismic systems are required to display a stable response under cyclic load, quantified as a maximum reduction of load capacity of 10%, according to the EN 15129 provisions [43].The application of dissipative devices as additional element to the anchors offers a contribution in this sense. D’Ayala and Paganoni, have developed a Dissipative Grouted Anchoring System (D-GAS) that could combine the availability of steel anchors and the energy dissipation capacity of a friction-base device [23]. This initial prototype has been refined

by D'Ayala & Melatti [24] after extensive testing, by introducing brass and FEP friction interfaces to control the variation of effective damping, and by optimising the shape of the slider to avoid stress concentration during the sliding motion. With a reduction of load capacity of 5% under cyclic loading, the device shows a performance well within the EN 15129 code requirements, even after exposure to adverse environmental conditions. A full assessment of the dissipative devices is reported in [24].

In this section, an equivalent non-linear model for the rocking of masonry walls is developed to derive a simplified capacity curve describing the performance associated to the out-of-plane (OOP) failure mode. An equivalent static assessment of the wall's capacity is performed comparing the displacement demands obtained through inelastic spectra to the limit displacement that the wall presents. The restrain afforded by connection to orthogonal walls is ignored in this model.

For walls vulnerable to OOP failure, the use of grouted anchoring systems is proposed to improve the seismic response of the wall. Both the Italian guidelines [15], which specifically addresses the retrofit of heritages structures and the EC8 [16], give little guidance regarding design procedures for anchorages in masonry walls. To the purpose of addressing such technical gap, a design procedure applicable to the GAS and D-GAS is here proposed.

In the model it is assumed that a vertical crack at the connection between front and side walls develops because of the seismic action both in the unstrengthened and strengthened configurations. However, the tying effect of anchors can cause a pseudo-diagonal crack involving a portion of the side wall. Experimental tests performed on strengthened connections [10, 36] have shown that the portion of side wall involved in the rocking motion is limited and it is therefore neglected in this study, as far as its mass is concerned. For what concerns the additional strength of the connection associated with the masonry bond the study assumes that the bond capacity is poor before and after the strengthening as shown by numerous post-earthquake evidences.

The contribution of the anchors is included in the model by an idealised non-linear constitutive law obtained from the load-strain curves presented in Section 2. The presence of the dissipative device is included by limiting the tensile capacity of the anchor to the sliding threshold of the device and by increasing the ultimate displacement capacity to account for the full capacity of the slider. Depending on the type and sizing of the strengthened configuration assumed, the displacement capacity of the wall and the inelastic seismic demand vary, and the design solution is not unique. Therefore, a dynamic analysis is proposed as a final step of the design procedure to validate the vulnerability assessment of walls prone to overturning and determine the optimal solution to strengthened them. Having computed the evolution of the system throughout the seismic event, the optimal solution is determined for the design that minimizes the sizing of the intervention and maximize the energy dissipated by the anchoring system with respect to the seismic energy imparted to the wall.

### 3.1 Static out-of-plane assessment of unstrengthened wall

Several procedures are available in literature to derive capacity curves for masonry structures. In the macro-element approach, the entire building is subdivided in a number of blocks which are identified by assuming a predefined crack pattern. D'Ayala [22] identified a set of 12 possible collapse mechanisms and used a kinematic approach to identify the collapse load multiplier (λ) that determines each collapse. The values λ are computed considering the geometry and materials of the selected building as obtained from site inspections and laboratory tests. The lowest value of λ identifies the mechanism that is more likely to happen for the selected building. Having converted the parameters of the selected mechanisms to those corresponding to an equivalent nonlinear SDOF system, the capacity curve of the idealized system is obtained [44].

In this work the load-displacement capacity of walls prone to one-sided rocking motion is computed considering an equilibrium limit analysis, following the procedure initially proposed by [45]. This approach allows to compute the ductility capacity of the system, and thereby to obtain a capacity curve which is then used to determine the performance points by intersection with inelastic demand spectra following the N2 approach [46] as recommended by the Eurocode 8 [16].

The non-linear model shown in Fig. 4 can be developed to determine the capacity of the system: the front wall (façade) is modelled as a single-degree-of-freedom (SDOF) block which can rotate on one side only and is subjected to dead loads, to horizontal seismic action. The equilibrium equation can be written as:

$$mg\,\mathrm{R_G}\sin(\beta_G - \theta) - mg\,u_\theta(\theta) = \lambda_\theta\, mgR_G\cos(\beta_G - \theta) \qquad (10)$$

where $R_G$ is the distance between the centroid *G* and the geometrical corner *O*, $g$ is the gravity acceleration, $m$ is the mass of the wall per unit of length, $\theta$ is the wall angular displacement, and $\beta$ is the *arctan (B/H)*.

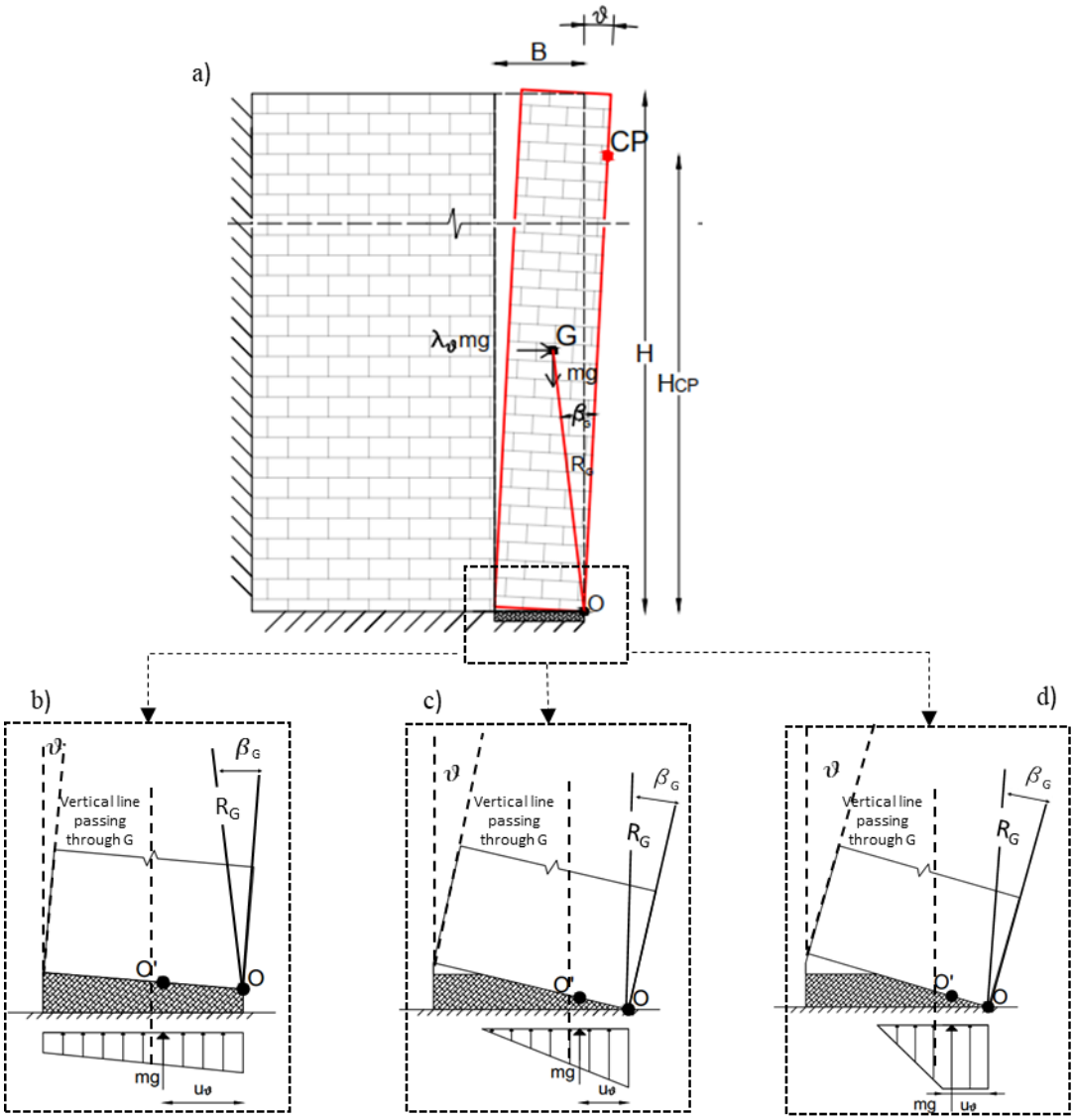


Fig. 4 One-sided displaced configuration of unstrengthened wall a) resting on a deformable interface of finite strength: evolution over rotation $\theta$ of interface stress distributions for (b) full contact, (c) partial contact and (d) toe-crushing (Figure adapted from [47])

To account for the finite stiffness of the foundation and of the block simulating the masonry wall, a flexible interface can be modelled at the base of the block, as proposed by [47–49]. Such interface has normal stiffness $k_n = E/e$ ($E$ = Young's modulus, $e$ = thickness of the interface), width $B$ equal to the thickness of the wall. The finite compressive strength $f'_m$ of the materials in contact is accounted for by considering the stress block of Fig. 4d.

The Eq. (10) considers equilibrium of moments around the instantaneous centre of rotation of the body O', which corresponds to the intersection of the base line of the block with the line of action of the stress block resultant at the base. As shown in Fig. 4, Point O' migrates from perfect alignment with the vertical line passing through the centroid G for $\theta = 0$, towards the geometrical edge O as $\theta$ increases. The inward shift of the rotation point determines a reduction of the stabilizing moment provided by the self-weight, as the lever arm reduces to the horizontal distance between the vertical lines passing through G and O', respectively. In Eq. (10) this reduction is accounted by the term $mg\, u_\theta(\theta)$, where $u_\theta(\theta)$ represents the distance between O' and O. Following Costa's approach [47] and with reference to Fig. 4, the position of the reaction force assumes different expressions as a function of the increasing value of the rotation θ:

$$u_\theta(\theta) = \begin{cases} \dfrac{B}{2} - \dfrac{B^3 k_n \theta}{12\, mg} & 0 < \theta \le \theta_{PC} \\ \dfrac{1}{3}\sqrt{\dfrac{2mg}{B^3 k_n \theta}} & \theta_{PC} < \theta \le \theta_{TC} \\ \dfrac{1}{2}\left(\dfrac{mg}{f_m} + \dfrac{f_m^3}{12\, mgk_n^2\theta^2}\right) & \theta \ge \theta_{TC} \end{cases} \tag{11}$$

Full contact is assumed for cases in which the rotation is less than the rotation $\theta_{PC}$ corresponding to partial contact of the base and given by Eq. (12):

$$\theta_{PC} = \frac{2mg}{B^2 k_n} \tag{12}$$

Beyond this point, horizontal cracks form on the left-hand side and only part of the cross section is in compression. Eq. (13) provides the rotation at which the toe-crushing failure occurs, namely the compressive stress is equal to the compressive strength of the masonry $f_m$ and vertical cracking occurs at the base on the right-hand side:

$$\theta_{TC} = \frac{f_m^2}{2k_n mg} \tag{13}$$

Solving Eq. (10) for incremental values of $\theta$ returns the capacity curve of the unstrengthened system shown in Fig. 5a, where the values of acceleration multiplier and horizontal displacement are normalized with respect to those of a wall resting on a rigid interface. The horizontal displacement refers to a Control Point (CP) arbitrarily identified at height $H_{CP}$ and are computed as:

$$\Delta = H_{CP} \tan\theta \tag{14}$$

The initial part of the curve is shown in detail in Fig. 5b to illustrate the stiffness reduction of the wall for relative displacements of CP greater than the one causing partial contact of the base $\Delta_{PC}$, and the decrement in capacity for $\Delta$ greater than the displacement at the toe-crushing failure at the wall's base $\Delta_{TF}$.

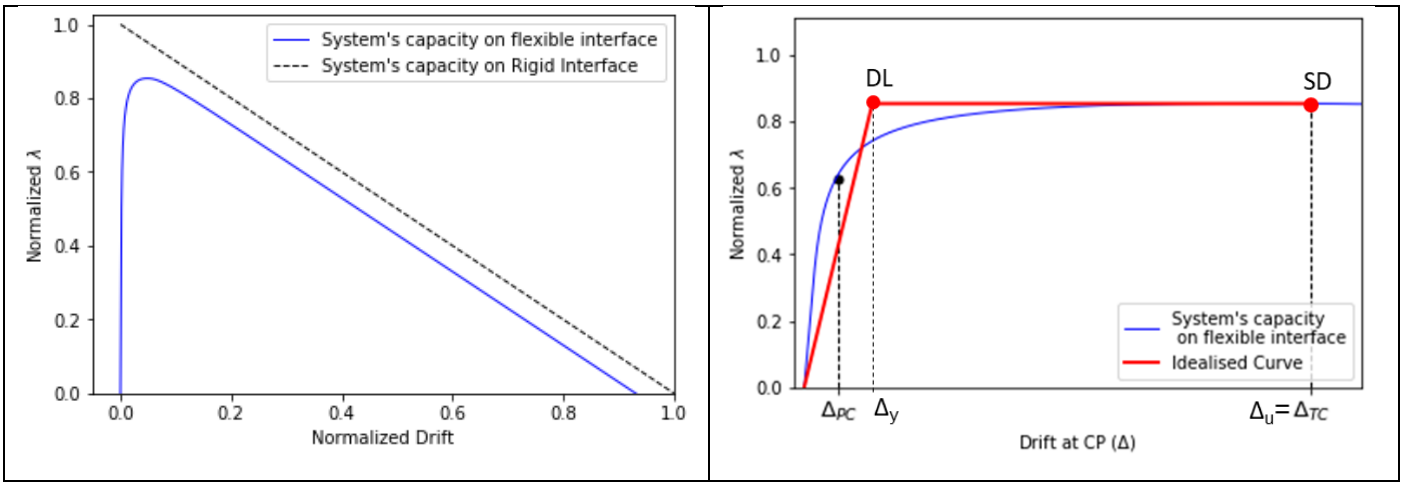


Fig. 5 a) Capacity curve of the unstrengthened wall resting on flexible interface b) with idealized capacity curve

The initial part of the curve is shown in detail in Fig. 5b to illustrate the reduction of the wall's stiffness for displacements greater than the one causing partial contact of the base $\Delta_{PC}$, and the decrement in capacity after the toe-crushing failure of the wall's base $\Delta_{TC}$.

For the obtained capacity curve, it is possible to identify a set of damage thresholds which refer to increasing level of damage in the system. According to the assessment procedure proposed by [50], these are defined as the states of Damage Limitation (DL) and of Significant Damage (SD), corresponding to the displacement when the system starts to degrade and reaches its ultimate deformation $\Delta u$. The damage thresholds are typically identified on a linearized elastic-perfectly plastic relationship which simplifies the behaviour of the real system up to its ultimate displacement $\Delta u$, set equal to $\Delta_{TC}$ for the unstrengthened wall. The idealized curve shown in Fig. 5b is obtained assuming that the linearized system will reach the same ultimate displacement $\Delta u$ and acceleration of the real one and imposing equal energy deformation for both systems. From the linearized system, the yielding point of coordinates $(\Delta_y, \lambda_y)$ is used to identify the limit state of DL and the elastic period $T^*$of the system can be deduced as:

$$T^* = 2\pi \sqrt{\frac{\Delta_y}{\lambda_y g}} \tag{15}$$

The term *yielding* is used with respect to the idealized curve to identify the beginning of the ductile phase of the linearised system.

This method provides a simple procedure to compute the capacity of an unstrengthened wall and defines the displacement thresholds corresponding to two damage levels for the system.

The seismic assessment of the system is then performed according to the N2 method, described in detail in the EC8. Here, it suffices to recall that the displacement demand for a predetermined Limit State (LS) depends on the displacement of the system at yielding $\Delta_y$ and on ductility demand $\mu_d$:

$$\Delta_{LS} = \mu_d \, \Delta_y \tag{16}$$

Where $\mu_d$ is function of the ratio between the spectral accelerations corresponding to the elastic and inelastic system, and of the value of elastic period $T^*$ with respect to $T_C$:

$$\mu_d = \begin{cases} \left(\frac{S_{ae}(T^*)}{S_{ay}} - 1\right)\frac{T_C}{T^*} + 1 & if\ T^* < T_c \\ \frac{S_{ae}(T^*)}{S_{ay}} & if\ T^* < T_c \end{cases} \tag{17}$$

The system is deemed safe if the seismic displacement demand $\Delta_{LS}$ is smaller than the displacement capacity associated to the damage levels.

If the performance of the system does not comply with the code requirements, the implementation of strengthening systems must be considered. In the next section, a grouted anchoring system (GAS) and an innovative dissipative anchoring system (D-GAS) are presented, and the contribution offered by these systems to the capacity of the wall is computed.

### 3.2 Static out-of-plane assessment of wall strengthened by GAS

Grouted anchors are typically installed to improve the connections of orthogonal wall in HMB, preventing the out-of-plane (OOP) separation of the masonry panels during a seismic event. Under the hypothesis that the wall remains in its perfectly vertical position for the PGA corresponding to an expected seismic action [15], the GAS and the wall are assumed to remain in their elastic/linear range. The force that the anchor must resist can be computed following a force-based approach and has to be checked against the maximum pull-out force $F_t$ that the anchor can sustain, according to the failure mode of the anchor.

A second design approach is to assume that the seismic force exceeds the anchor capacity and that an OOP mechanism develops.

In this case, the non-linear model presented for the unstrengthened wall is modified to consider the restraining action $F_{AS,i}$ provided by each anchor placed at height $H_{t,i}$ from the base of the wall. With reference to Fig. 6 the equilibrium equation of the wall strengthened by GAS is presented in Eq. (18):

$$mg\,\mathrm{R_G}\sin(\beta_G - \theta) - mg\,u_\theta(\theta) + \sum_1^n F_{AS,i}\,R_{AS,i}\cos\left(\beta_{AS,i} - \theta\right) = \lambda_\theta\, mgR_G\cos(\beta_G - \theta) \tag{18}$$

a) b)

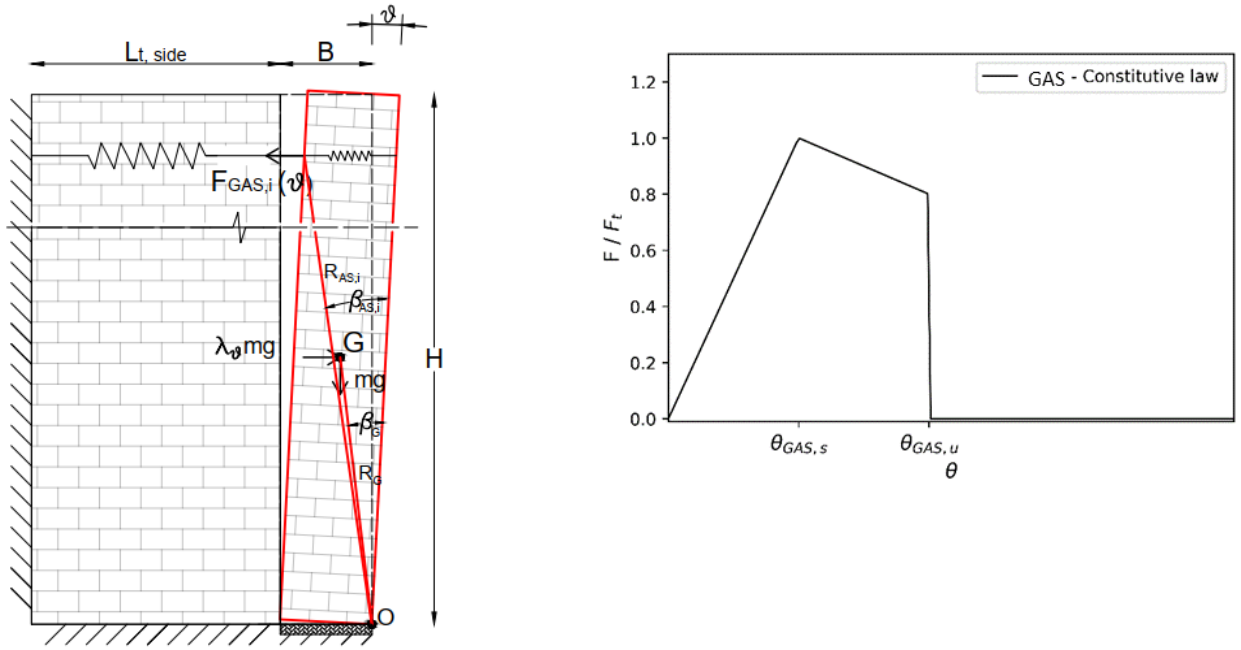


Fig. 6 a) One-sided displaced configuration of a wall restrained by a GAS, b) Idealized monotonic behaviour of grouted anchors for increasing rotations

This model assumes that, as a result of a capacity design process, no failure in the adjacent masonry wall occurs and that no change of mechanism takes place, from single body to multi-bodies [20,51]. Moreover, the model assumes that the bond strength of the portion of anchor grouted in the side wall is significantly higher than the one grouted in the front due to a longer embedment length. For this reason, the former is considered as fixed and does not participate in preventing the out-of-plane motion. This assumption is justified by experimental results as reported by [10, 12, 36].

The restoring action provided by the GAS is characterized by its slip strain ($\varepsilon_s = 0.005$) and ultimate strain ($\varepsilon_u = 0.01$) obtained in section 2 based on the slip $d_s$ and ultimate elongation ($d_s$ and $d_u$) of grouted anchors obtained by pull-out tests, assuming also for the tie a bilinear behaviour. The rotations thresholds corresponding to the maximum and ultimate load capacity are computed respectively as:

$$\theta_{GAS,s} = \tan^{-1}\frac{\mathrm{d_s}}{H_{t,i}} = \tan^{-1}\frac{\varepsilon_s \; l_e}{H_{t,i}} \tag{19}$$

$$\theta_{GAS,u} = \tan^{-1}\frac{\mathrm{d_u}}{H_{t,i}} = \tan^{-1}\frac{\varepsilon_u \; l_e}{H_{t,i}} \tag{20}$$

where $l_e$ is the effective embedment length, namely the thickness of the front wall, as a vertical crack is assumed, and $H_{t,i}$ is the tie's installation height. The ultimate load is computed as the 80% of $F_t$, in accordance with the convention adopted for the experimental database in section 2 [35]. An idealized relationship between $F_{AS}$ and $\theta$ is obtained considering that the force increases linearly up to the slip rotation $\theta_s$, experiences a linear degradation up to $\theta_u$ and then then drops to 0, as shown in Fig. 6b, and formalized by the set of Eq.(21):

$$F_{AS}(\theta) = F_{GAS}(\theta) = \begin{cases} \dfrac{F_t}{\theta_{GAS,s}}\theta & 0 < \theta \le \theta_{GAS,s} \\ F_t\left(1 - 0.2\dfrac{\theta - \theta_{GAS,s}}{(\theta_{GAS,u} - \theta_{GAS,s})}\right) & \theta_{GAS,s} \le \theta \le \theta_{GAS,u} \\ 0 & \theta \ge \theta_{GAS,u} \end{cases} \tag{21}$$

The anchoring system is designed as the first component to fail, meaning that it will reach the ultimate rotation $\theta_{GAS,u}$ before the toe-crushing failure occurs at $\theta_{TC}$. This condition is shown in Fig. 7 where the capacity curve of a wall strengthened by two GAS is presented in terms of horizontal displacement of the control point and normalized acceleration multiplier: the anchors largely increase the load capacity of the system up to the displacement $\Delta_{GAS,u}$ after which the overturning moment is balanced by the self-weight of the wall only, as it was for the case of unstrengthened walls. Because of this sudden loss in capacity, it can be considered that the ultimate deformation $\Delta u$ for the "wall-with-GAS" system corresponds to the failure of the topmost anchor. This assumption can be perceived as excessively conservative in case several anchors are distributed along the height of the wall and a greater total deformation is available. Indeed, it could be assumed that the bond failure of the lower anchor is governing the ultimate displacement

of the rocking wall. However, the purpose of the anchors should be to remain integral while controlling the deformation of the wall to limit excessive damage to the structure. Therefore, the choice of $\Delta u$ is justified in this context, even though it might be conservative. On this assumption, the idealized curve and the damage states are obtained, as shown in Fig. 7 and the ductility capacity of the strengthened system is computed as:

$$\mu_c = \frac{\Delta_u}{\Delta_y} \tag{22}$$

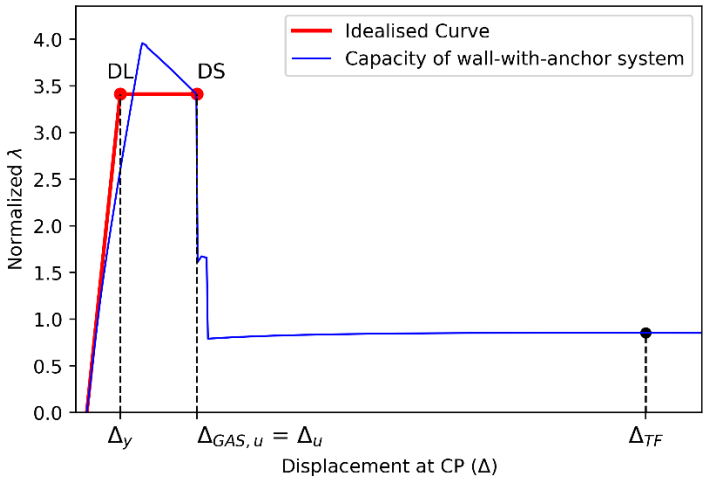


Fig. 7 Capacity curve of the "wall-with-GAS" system, including idealized capacity curve and damage limit states

Despite the large load capacity offered by the GAS, the anchoring system displays a reduced ductile behaviour between yielding and failure. Moreover, the horizontal path does not refer to the yielding of the steel rebar, which would offer a longer ductile behaviour, but of the brittle debonding of the grout from the surrounding masonry according to the most recurring failure modes highlighted in section 2.3. Therefore, the use of the dissipative device, able to provide a larger ductile behaviour becomes imperative to improve the seismic performance of such systems.

### 3.3 Static analysis of wall strengthened by D-GAS

The insertion of a Dissipative Grouted Anchoring System (D-GAS) at the connection between perpendicular walls (Fig. 8a) determines that the friction-based device (Fig. 8b) allows for a controlled displacement of the out-of-plane wall.

a) b)


Fig. 8. a) insertion of dissipative anchoring system at the connection between orthogonal walls, b) friction-based device

The system is schematically represented in Fig. 9b by a system of springs and a slider representing the grouted anchors and the device, respectively. The strength of the grouted ties, $F_{bond,side}$ and $F_{bond,front}$, is determined considering the capacity of the bond strength developed between the ties and the parent material. According to the failure modes observed for grouted anchors, a load bearing capacity of each anchor's portion is assumed according to the set of equations proposed in section 2.3.

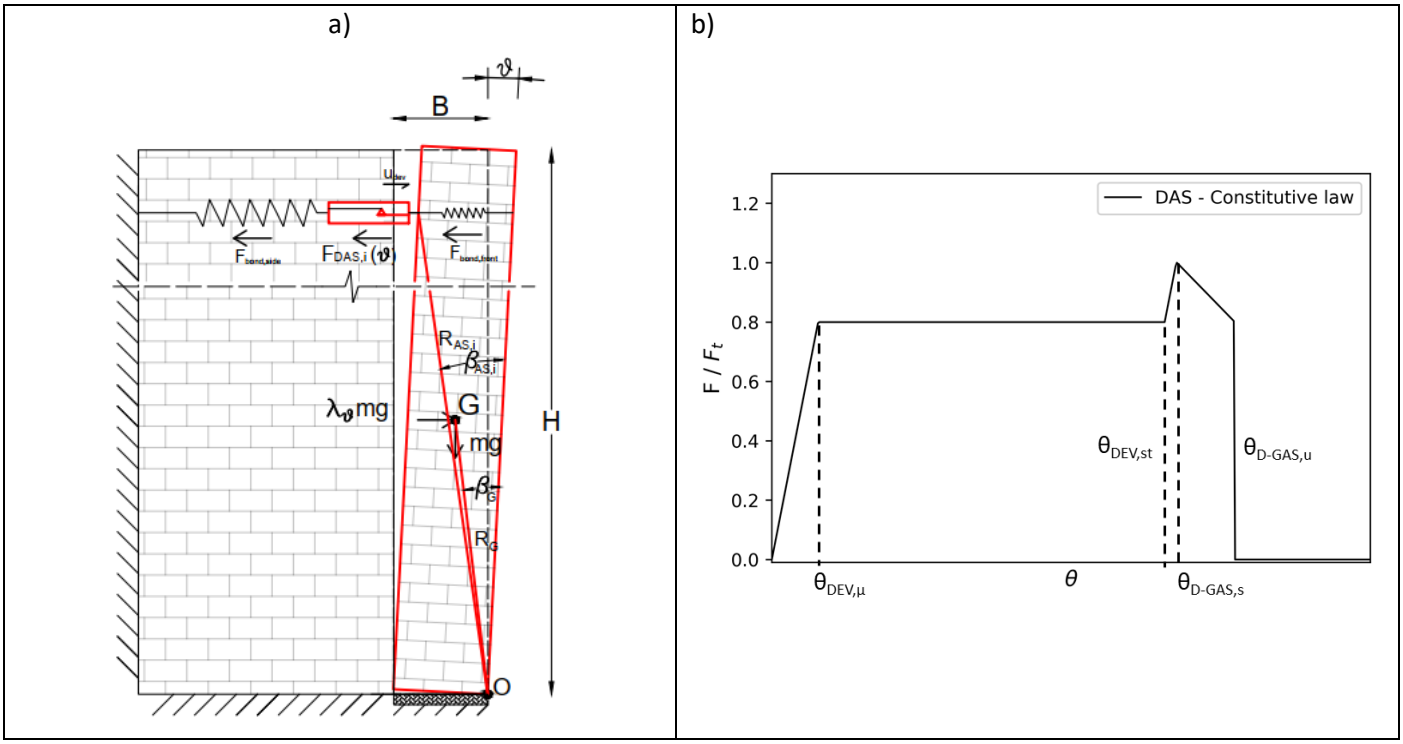


Fig. 9 a) One-sided displaced configuration of a wall restrained by a D-GAS, b) Idealized monotonic behaviour of D-GAS for increasing rotations

Conversely, the slippage load at which the device activates is equal to the friction resistance $F_{\text{fric}}$ the device is designed to provide. The system is adjusted to have $F_{\text{fric}}$ at the bottom of the anchor strength hierarchy, so that, during an earthquake, the detachment of the façade from the side walls triggers the activation of the device and prevents the pull-out failure of the anchors. Therefore, the device is tuned to activate for a slippage load smaller than the bond that the two grouted steel elements can provide. The strength design check is expressed by Eq. (23) :

$$F_{\text{fric}} < \min\left(F_{bond,side}, F_{bond,front}\right) \tag{23}$$

The D-GAS can be installed along the wall height, so that the energy dissipation can take place even for small rotations of the rocking motion. It is suitable both for connections that have already experienced a crack as a result of a seismic event or for undamaged connections which are deemed to have poor bond between façade and side walls. In the latter case, a structural analysis is required to determine the optimal location for the device, namely whether a vertical or diagonal crack is likely to occur. As for the case of the GAS, it is here assumed that a vertical crack develops at the interface between walls. The presence of the device reduces the stiffness of the connection when the imposed load exceeds the slippage load facilitating the crack propagation and reducing the portion of spine wall involved in the motion [26].

The sliding motion is bounded to a maximum displacement by a steel solid pin, with strength capacity greater than the anchor bond strength, and results in the dissipation of the input seismic energy. Once the maximum allowable run $\Delta u_{\text{dev}}$ is achieved, the system behaves like a grouted anchor up to ultimate failure, as shown in Fig. 9b. Considering the combined ductility of anchor and device, the capacity of a wall restrained by D-GAS is assessed on a Displacement-based approach, computing the force provided by the D-GAS for increasing rotations:

$$F_{AS}(\theta) = F_{D-GAS}(\theta) = \begin{cases} \dfrac{F_t}{\theta_{GAS,s}}\theta & if\ 0 < \theta \le \theta_{\text{DEV},\mu} \\ F_t\, C_{D-GAS} & if\ \theta_{\text{DEV},\mu} \le \theta < \theta_{\text{DEV,st}} \\ F_t\, C_{DAS} + \dfrac{F_t}{\theta_{GAS,s}}\left(\theta - \theta_{\text{DEV,u}}\right) & if\ \theta_{\text{DEV,st}} \le \theta < \theta_{D-GAS,s} \\ F_t\left(1 - 0.2\dfrac{\theta - \theta_{D-GAS,s}}{(\theta_{D-GAS,u} - \theta_{D-GAS,s})}\right) & \theta_{D-GAS,s} \le \theta \le \theta_{D-GAS,u} \end{cases} \tag{24}$$

$C_{D-GAS}$ is the activation coefficient of the D-GAS. It varies between 0 and 1 (excluding the extreme points) and determines the device's slippage force as a fraction of the anchor's capacity $F_t$. The rotation at which the device

activates, $\theta_{\mathrm{DEV},\mu}$ and stops, $\theta_{\mathrm{DEV,st}}$, and the rotations at which the D-GAS reaches its maximum and ultimate capacity ($\theta_{D-GAS,s}$ and $\theta_{D-GAS,u}$ are obtained as:

$$\begin{aligned}\theta_{\mathrm{DEV},\mu} &= \theta_s C_{D-GAS}\\ \theta_{\mathrm{DEV,st}} &= \theta_{\mathrm{DEV},\mu} + \arctan\left(\frac{\Delta u_{DEV}}{H_t}\right)\\ \theta_{D-GAS,s} &= \theta_{GAS,s} + \arctan\left(\frac{\Delta u_{DEV}}{H_t}\right)\\ \theta_{D-GAS,u} &= \theta_{GAS,u} + \arctan\left(\frac{\Delta u_{DEV}}{H_t}\right)\end{aligned} \tag{25}$$

For incremental rotation of the wall's base, the ultimate rotation of the D-GAS $\theta_{D-GAS,u}$ must precede the toe-crushing failure of the wall's base, to preserve the integrity of the wall. This condition is formally expressed as:

$$\theta_{GAS,u} + \arctan\left(\frac{\Delta u_{DEV}}{H_t}\right) < \theta_{TC} \tag{26}$$

Which allows computing the allowable sliding capacity of the dissipative device once $\theta_{TC}$ is determined. The improvement in displacement between the two systems is quantified by the ratio, η, between the respective ultimate rotations:

$$\eta = \theta_{D-GAS,u}/\theta_{GAS,u} \tag{27}$$

The capacity curve for the "wall-with-D-GAS" system is shown in Fig. 10a for the case of two D-GAS with $C_{D-GAS}$ set at 0.7. The idealized curve obtained considering that the system has the same ultimate displacement and acceleration capacity of the real one, may not be a good approximation of the anchor's behaviour, as it may result in a significant reduction of the elastic stiffness and overestimation of the load capacity. Instead, the optimized bilinear curve shown in Fig. 10a can be considered minimizing the difference in elastic stiffness *K* and ultimate acceleration multiplier $\lambda$ between the optimized (index "O"), the real (index "R") and the ideal system (index "I"):

$$\min(\Delta K_{o-R} - \Delta\lambda_{O-I}) = \min\left(abs\left(\frac{K_O - K_R}{K_R}\right) - abs\left(\frac{\lambda_{u,O} - \lambda_{u,I}}{\lambda_{u,I}}\right)\right) \tag{28}$$

By singularly plotting the difference in stiffness and acceleration multiplier ($\Delta K_{o-R}$ and $\Delta\lambda_{O-I}$) it is possible to identify the optimal stiffness and ultimate acceleration multiplier ($K_O$ , $\lambda_{u,O}$) as the intersecting point of the two curves, as shown in Fig. 10b. From this, the yielding displacement $\Delta_y$ is easily computed as:

$$\Delta_y = \frac{\lambda_y}{K_O} = \frac{\lambda_{u,O}}{K_O} \tag{29}$$

On the graph shown in Fig. 10b, the optimal point is close to the parameters corresponding to the "real behaviour" of the system, meaning that optimized curve provides a better approximation of the actual system's capacity. For this reason, the damage limit states are identified for the yielding and ultimate points of the optimized curve rather than on the idealized one.

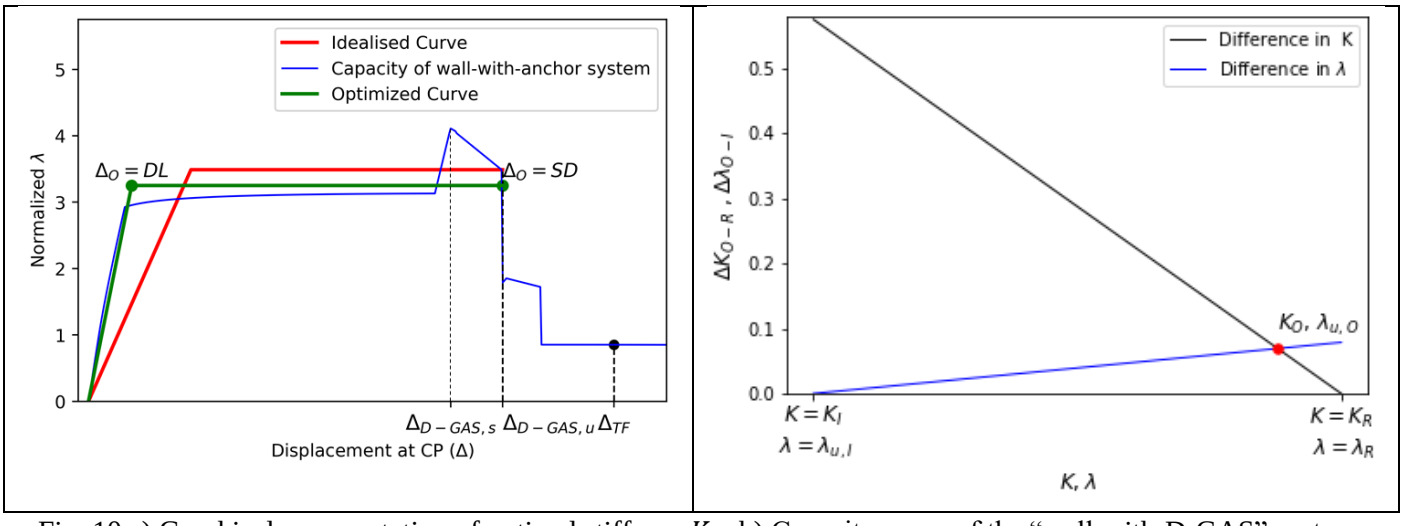


Fig. 10 a) Graphical representation of optimal stiffness $K_O$, b) Capacity curve of the "wall-with-D-GAS" system, including damage limit states

Comparing the capacity curves obtained for the unstrengthened and strengthened walls, it can be concluded that the implementation of the D-GAS improves both the load and ductility capacity of the system. The design of the GAS and D-GAS according to the N2 method would require dimensioning the number and sizing of the system ensuring that the expected seismic performance does not exceed the capacity. Nonetheless, this static procedure might overlook some critical aspects of the behaviour of walls during seismic events. A critical aspect concerns the computation of the inelastic displacement demand, obtained by Eq. (16) according to the value of expected ductility (Eq. (32)). This relation is appropriate for several typologies of structures, such as reinforced concrete frames with masonry infills [50], and needs to be verified for the simplified model of wall restrained by anchorages proposed in this study. This can be achieved verifying that the displacement demand predicted by the static analysis is close to the horizontal displacement experienced by the system for a corresponding ground motion. Therefore, in the next paragraph a dynamic analysis of the wall in different configurations is proposed to validate the results of the assessment and design procedure proposed in this work.

### 3.4 Non-linear Time-history analysis

The Displacement-based procedure proposed allows assessing the vulnerability of historical masonry walls to out-of-plane failure, verifying the safety of the macro-element to an expected seismic action. If the performance does not comply with the code limits, the N2 method is extended to make it applicable to wall strengthened by traditional and dissipative anchoring systems.

Nonetheless, this equivalent static procedure neglects relevant aspects of the motion, such as the evolution of the system over time and the dissipated energy. By contrast, a nonlinear dynamic analysis fully considers the evolution of motion and the effect of inertial forces during reversal loads such as seismic actions. Hence, to determine a more accurate response of the system in original and strengthened configuration, verify the assumptions made in the static analysis, and the effectiveness of the proposed seismic strengthening, the structural behaviour is investigated by means of nonlinear time-history analyses.

A numerical approach can be set out by extending the assumptions and constraint used to derive the limit static behaviour, represented by Eq. (10), to the dynamics motion resulting by subjecting the walls to a seismic input. Adapting the classical equation of rigid body rocking [52] to the present case of one-side rocking, the equation reads as follows:

$$\ddot{\theta}(t) + p_\theta^2 \left[ \sin\big(\alpha - \theta(t)\big) - \frac{u_\theta}{R_G} + \sum_1^n F_{AS}(t)\, H_{t,i} \frac{cos\theta(t)}{mgR_G} + \frac{\ddot{u}_g}{g} \cos[\,\alpha - \theta(t)] \right] = 0 \tag{30}$$

where $p_\theta = \sqrt{mgR_G/I_\theta}$ is the frequency parameter, $I_\theta$ is the polar moment of inertia of the wall with respect to the instantaneous centre of rotation O', and $R_G$ is the distance between the body centroid and O'. Similar to the kinematic approach, the presence of $n$ anchors at heights $H_{t,i}$ is taken into consideration by adding their contributions as a stabilizing moment opposing the overturning moment produced by the base acceleration.

When the block is in motion it will dissipate energy at every impact with the side wall and the foundation. Al Shawa et al. [53] propose a coefficient of restitution for the case of a façade laterally restrained on one side by transverse walls to account for the energy dissipated at impact. The value of $e$ is obtained considering that within one rebound the front wall impacts twice with the base and once with the side wall in different - but close in time – instants. Imposing the conservation of momentum, the coefficient of restitution is obtained as the combination of the three impacts:

$$e = -1.05\, e_f e_{tr} e_f = 1.05 \left(1 - \frac{3}{2}\sin^2 \vartheta_c\right)^2 \left(1 - \frac{3}{2}\cos^2 \vartheta_c\right) \tag{31}$$

where the coefficient 1.05 was determined experimentally and the minus implies a rebound after the impact. With the obtained value of $e$ it is possible to numerically solve Eq. (30) to perform a nonlinear time history analysis alternative to equivalent static procedures for the assessment of HMB [19].

To compare the static and dynamic results, a spectrum-compatible accelerogram is used as ground motion acceleration in Eq. (30). Because real accelerograms have specific frequency and amplification content and are not directly related to the code-defined design spectrum, spectrum-compatible accelerograms can be obtained, based on the modification of actual ground motions. Several methods have been proposed in literature to generate spectrum-compatible accelerograms. In this work, the code developed by [54] is used: it determines the response spectrum of the accelerogram and returns its best fit to the design spectrum locally relevant. This procedure allows the use of a single accelerogram to induce an inelastic response consistent with the design scenario defined by the appropriate code, rather than running several analyses to account for the inherent hazard uncertainty and limitation associated with considering an individual accelerogram.

From Eq. (30) it is clear that solving the equation of motion for $n = 0$ returns the dynamic response of the original structure. This can be compared to the performance predicted by the static procedure to determine the validity of

whether the elastic or secant period gives the best approximation of the displacement demand for a selected seismic action.

The presence of the GAS and D-GAS is included by selecting the appropriate constitutive law between Eq.(21) and Eq. (24) to be used in place of $F_{AS}$. For both strengthening systems, the proposed DB design takes into consideration their ductility, i.e. the hysteretic energy dissipation of ductile structures, to reduce the seismic demand and compute the performance of the system. Solving the equation of motion of the strengthening systems permits the direct comparison between maximum horizontal displacement experienced by the rocking wall $\Delta_{max,rk}$ and the deformation that the system is expected to display according to the static procedure for a selected limit state $\Delta_{LS}$. The variation between static and dynamic maximum displacement is expressed by the following ratio:

$$\beta = \frac{\Delta_{LS}}{\Delta_{max,rk}} \tag{32}$$

For values of $\beta$ close to unit it can be assumed that the $\mu - T$ relation provided by the code [16] gives a good approximation of the dissipative energy of the system and that the use of Eq. (16) and (32) can be extended to the case of walls strengthened by anchors.

Moreover, the dynamic analysis can be used as a supplementary tool to design method to determine the optimal design solution, comparing the energy dissipated by the each strengthening system $E_D$ with respect to the seismic energy $E_I$ imparted to the structure during the seismic action. The ration $\gamma$ is therefore computed as:

$$\gamma = \frac{E_D}{E_I} = \frac{\int_0^{S_T} F_t \, ds_T}{\int_0^{S_G} m\ddot{u}_g(t) \, ds_G} = \frac{\int_0^{T} F_t \, \dot{s}_T(t) \, dt}{\int_0^{T} m\ddot{u}_g(t) \, \dot{\theta}(t) \, R \, dt} \tag{33}$$

Where T is the duration of motion, $\dot{\theta}(t)$ is the angular velocity and $s_G$ and $s_T$ are the displacement experienced by the center of mass and the anchor, respectively.

In the next section, the assessment and design method is applied to a case study structure in need of seismic upgrade. Having determined its vulnerability to out-of-plane failure, a design scheme for the implementation of traditional and innovative anchoring solutions is proposed and the optimal design solution is justified by dynamic analysis.

## 4 Application of the design procedure to a case study

The previous section presented a SDOF model to assess the detachment and eventually the OOP failure of a wall subjected to seismic action. The model can include the presence of grouted anchoring systems (GAS) able to increase the load-bearing capacity of the wall, and of dissipative anchoring system (D-GAS), which additionally increase the displacement and energy dissipation capacity of the strengthened wall. Either static or dynamic analyses can be performed to determine whether the wall will experience OOP movement for a selected seismic acceleration and the best strengthening strategy to balance the overturning motion and prevent extensive damages to the structure.

The oratory of San Giuseppe dei Minimi, a church that suffered severe damage during the 6.3-magnitude earthquake occurred in L'Aquila (IT) in 2009 , is selected as case-study to discuss the validity of the presented model and the benefit of introducing a dissipative system into a wall prone to overturning. The structure displayed a clear pseudo-vertical crack opening at the interface between the façade's quoins and the rubble masonry of the side walls, with the upper portion of façade tilting forward as a whole, as visible from Fig. 11a. This failure mechanism, commonly observed in many historical buildings after the 2009 earthquake [1], is typical of façade walls with poor connection with the orthogonal walls and causes them to behave independently from the rest of the building [4]. Therefore, the selected case study is an ideal candidate for the implementation of grouted anchoring system, which restores the interaction between orthogonal walls.

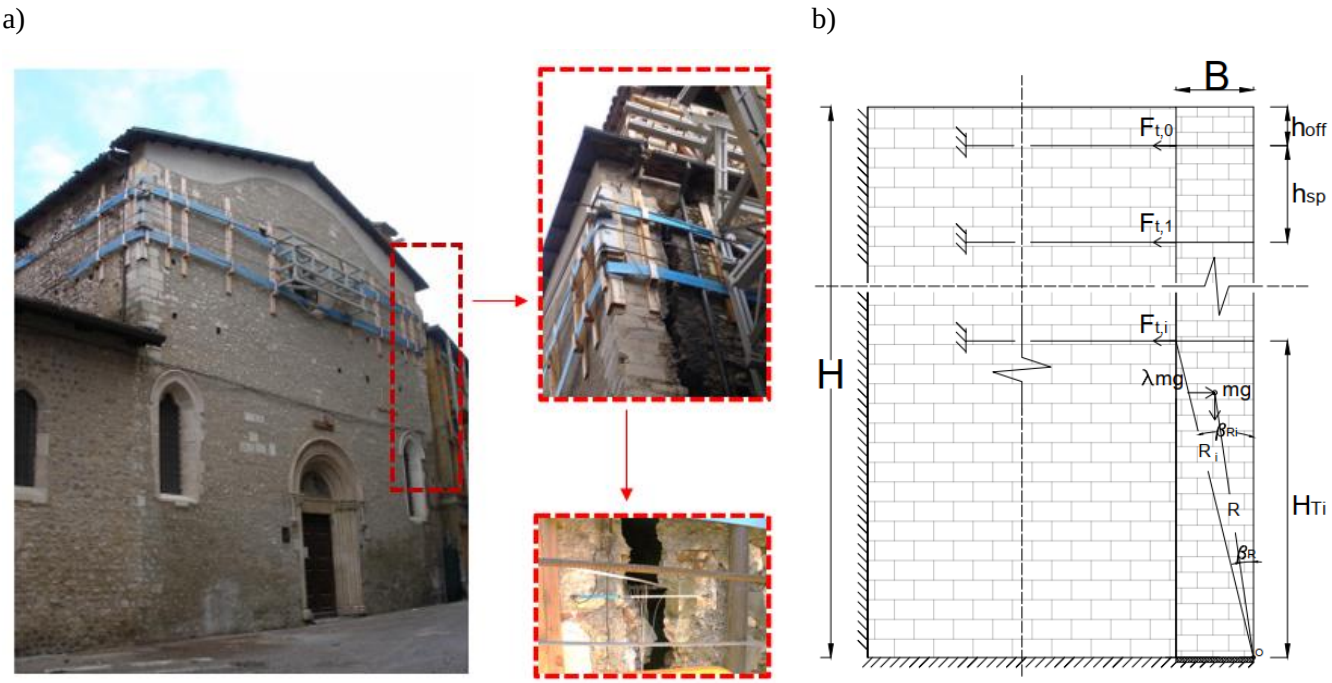


Fig. 11. The oratory of S. Giuseppe dei Minimi in L'Aquila, Italy. The crack between the front wall and side walls as seen from the outside, (b) representation of the façade as restrained by three anchors

The façade is modelled as a single rigid element able to rotate around a base hinge, according to the geometrical dimensions of the church reported by [26,55]. The presence of openings cannot be included in the model as the block geometry is 2-dimensional and the length of the wall is considered only to compute the mass participating to the motion. The mechanical properties of the masonry, shown in Table 3 as obtained by [26], are used to model the elastic interface that determines the initial stiffness of the wall and the rotation corresponding to the toe-crushing due to the compression limit strength. The results of the static and dynamic analysis in terms of OOP displacement are compared to the damage observed for the structure in the aftermath of the seismic event to determine the ability of the model to capture the typology and extent of the damage.

Table 3. Dimensions and mechanical properties of materials of the façade

| Façade Geometry | | | | Mechanical properties | | |
|---|---|---|---|---|---|---|
| Base<br>**B**<br>[m] | Height<br>**H**<br>[m] | Length<br>**$L_h$**<br>[m] | Mass Density<br>**ρ**<br>[KN/m$^3$] | Compressive Strength<br>**$f_m$**<br>[MPa] | Young modulus<br>**E**<br>[MPa] | Interface stiffness<br>**$k_n$**<br>[MPa] |
| 1 | 12.5 | 13.7 | 20.3 | 3.2 | 1020 | 6.6 |

The two strengthening options, GAS and D-GAS, discussed in the previous section, are designed and tested to determine the optimal strengthening solution. Regarding the anchoring typology, the technology developed by Cintec's is considered both for the GAS and D-GAS as it is widely used to restore HMB and has large load capacity. The anchors are installed at the corner connection between the façade and the orthogonal walls and are dimensioned according to the geometry of the structure and mechanical characteristic of the materials, which are indicated in Table 4. The force-based design is firstly considered to determine the number of anchors to be used and their location along the height of the wall. A symmetrical distribution of the anchors on the two sides of the façade and a constant vertical spacing between anchors is assumed. The location of the top-most anchor is selected as control point (CP) as it will experience the largest displacements. For sake of comparison between original and strengthened configuration, all displacements are computed with respect to the same CP in the three configurations. It should be noted that prior to implementing grouted anchors to restore the global integrity of the structure, localized intervention aimed at improving the mechanical characteristics of the masonry should be implemented, if necessary. Mortar injections, deep repointing or the insertion of transversal connectors can improve the shear strength and the in-plane stiffness of the walls, allowing the anchors to develop sufficient mechanical bonding with the substrate and thus the expected load capacity.

Table 4. Dimensions and mechanical properties of grouted anchors

| Anchor diameter | Hole diameter | Embedment length | Distance from top | Anchor spacing | Reduction factor | Grout compressive strength | Grout/masonry Bond | Elastic constant | Mass participation factor | Behaviour factor |
|---|---|---|---|---|---|---|---|---|---|---|
| $d_b$ [mm] | $d_h$ [mm] | $l_e$ [mm] | $h_{off}$ [mm] | $h_{sp}$ [mm] | $\phi_j$ [-] | $f_{c,g}$ [MPa] | $\tau_0$ [MPa] | $\lambda'$ [-] | e* [-] | q [-] |
| 16 | 50 | 4000 | 800 | 1000 | 0.5 | 50 | 2.5 | 0.51 | 1 | 2 |

The parameters defining the seismicity of the L'Aquila region according to the Eurocode 8 [16] are reported in Table 5. These are used to build the design spectra for the Damage and Ultimate limit states, DLS and ULS. The compliance of the structural response with the inelastic seismic demand corresponding to the two limit states is verified in the static analysis.

Table 5. Parameters defining the seismicity of the considered zone.

| PARAMETERS | Earthquake return period | Peak ground acceleration | Site response coefficient | Confidence Factor | Corner Period |
|---|---|---|---|---|---|
| | $T_R$ [years] | $a_g$ [g] | S [-] | $C_f$ [-] | Tc [s] |
| DAMAGE LIMIT STATE (DLS) | 50 | 0.104 | 1.57 | 1 | 0.44 |
| ULTIMATE LIMIT STATE (ULS) | 475 | 0.26 | 1.57 | 1 | 0.51 |

The accelerogram of the main shock of the 2009 earthquake (as recorded at the station of L'Aquila, Valle Aterno, Centro Valle, station code AQV) is adapted to fit the design spectrum for each limit state and used as input for the time-history analysis. The obtained accelerograms and spectra are reported in Fig. 12.

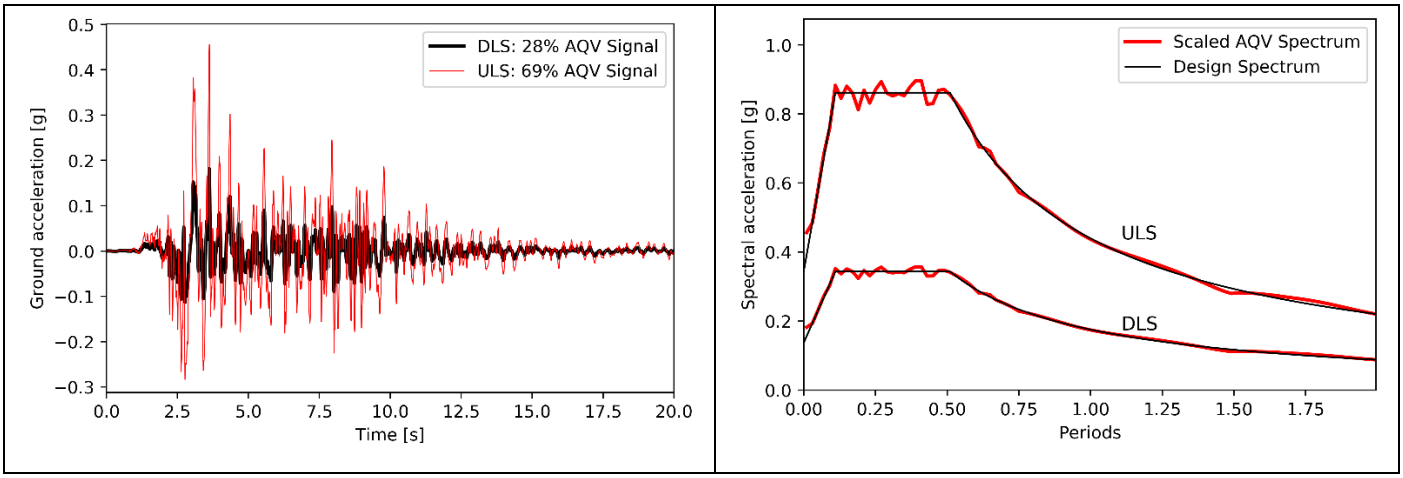


Fig. 12 Adaptation of the AQV earthquake signal according to the design spectra for (a) Damage Limitation and (b) Severe Damage limit states

### 4.1 Seismic performance of the original structure – Static analysis

The static assessment procedure introduced in Section 3 is adopted to evaluate the capacity of the wall in the original configuration and its safety for a selected seismic action. The elastic and inelastic demand spectra are computed for the values reported in Table 5corresponding to the Damage and Ultimate limit states (DLS and ULS) and the performance points are obtained by their intersection with the capacity curve, as illustrated in Fig. 13a for the ULS. These demand thresholds represent the displacement demand that the system needs to verify for the selected seismic action.

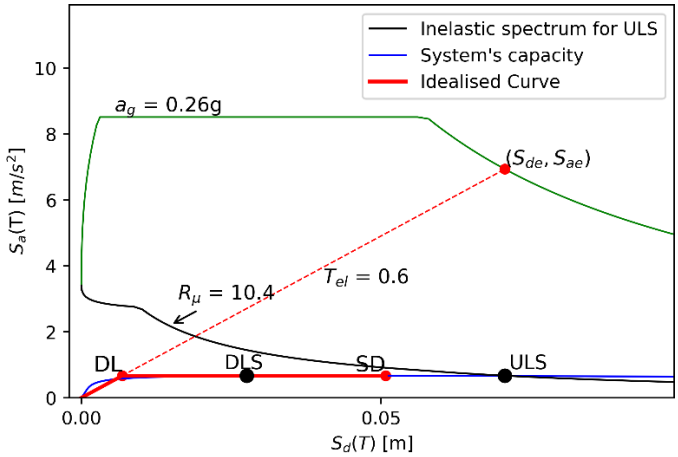


Fig. 13 Performance points corresponding to the DL and SD limit state for the wall in the unstrengthened configuration.

With reference to Fig. 13, the following results are obtained. From the idealized capacity curve, the elastic period $T^* = 0.6s$ is obtained. As it is larger than $T_C = 0.51\ s$, the "equal displacement rule" applies, namely the displacement of the inelastic system is equal to the displacement of the corresponding elastic one with the same period [46].

Thus, the displacement demand is $S_d = 0.027m$ and $S_d = S_{de}(T^*) = 0.07\ m$ andfor the DLS and ULS respectively. At the ULS, the displacement demand is larger than the displacement that causes the toe-crushing failure of the wall's base, meaning that the structure will suffer severe damage in case of a seismic event with magnitude similar to the one considered for the ULS limit state. The wall will suffer damages even for earthquakes of smaller magnitude, as the performance point corresponding to the DLS falls beyond the elastic capacity of the wall.

From the analysis's results, it can be concluded that the façade of the church will experience the detachment from the side walls and toe-crushing failure will occur at the wall's base for the for the considered seismic event at ULS. Nonetheless, the wall is not expected to overturn as the vertical line passing through the centre of mass falls within the wall's base for the maximum estimated value of displacement. This finds correspondence with the damages observed during site inspections, as already discussed with reference to Fig. 11a. After the detachment, the wall is likely to undergo rocking motion, changing direction of rotation depending on the direction of the seismic acceleration and of the inertial forces. The dynamic evolution of the damage can be predicted performing a time-history analysis, which is presented in section 4.4.

To reduce the vulnerability of the wall to OOP failure and protect its integrity, the implementation of traditional and innovative anchoring system is proposed in the next section and the improvement in seismic performance is determined.

### 4.2 Seismic performance of the structure strengthened by GAS

As shown in the previous section, the structure's seismic performance is inadequate, and therefore the implementation of seismic strengthening is necessary. As previously discussed, it is decided to use a set of grouted anchors to control the OOP mechanism. Initially, the GAS is dimensioned according to the Force-based procedure presented in Section 3.1. From the parameters defined Table 4 and Table 5, the load multiplier that determines the collapse mechanism is computed as:

$$\lambda_0 = \frac{a_{g(ULS)} S\, e^*}{q} = 0.27 \tag{34}$$

The maximum load that the GAS can provide is bounded by the bonding resistance of the front portion of the anchor, as provided by the smaller value between Eq. (6), (7), and (8) using the set of constants obtained for this work and reported in section 2.3:

$$F_t = min(90\ KN, 86KN, 140\ KN) = 86\ KN \tag{35}$$

For the considered mechanical properties of the masonry and the geometrical dimensions of the anchor, it is obtained that the design load is computed for the GSM failure mode. The larger value obtained by Eq. (8) is simply explained considering that the set of constants for the MIX mode is obtained for anchors with embedment length significantly smaller than the one available for the case study. The number of anchors $n$ is found solving the equilibrium equation given in Eq. (10) for $\theta = 0$ and $\lambda_\theta = \lambda_0$. It is found that 3 anchors are needed to ensure that the anchoring system does not fail for the design seismic action.

The design of the anchoring systems obtained following the FB method, namely three anchors are considered on each side to restrain the out-of-plane motion, is checked computing the capacity of the strengthened system for incremental base rotations and then comparing it with the seismic demand expected for the site.

The strengthening system is effective for the seismic action associated to the DLS, as the performance point falls within the elastic capacity of the anchor. On the other hand, the ductility demand $\mu_d = 3.9$ corresponding to the SD is larger than the ductility capacity of the grouted anchor ($\mu_c = 3.1$), and the displacement demand would cause the failure of the anchors. With the failure of the topmost anchor, the capacity of the system significantly reduces as the anchors at the highest location provide the larger contribution to the stabilizing moment. The evolution of the system can be investigated by dynamic analysis to determine if the wall would incur in cracking of the base for toe-crush failure, marked as "TF" in Fig. 14, after the anchor's failure.

To improve the seismic behaviour, the number of anchors is increased to 4 on each side. As illustrated in Fig. 14b, the design is now adequate to provide enough strength to reduce the ductility demand. Nonetheless the feasibility of the intervention is ultimately regulated by the principles of minimum intervention and non-intrusiveness enshrined in the ICOMOS/ISCARSAH chart [56], as the larger number of anchors to be core-drilled into the walls might compromise the integrity of the original material.

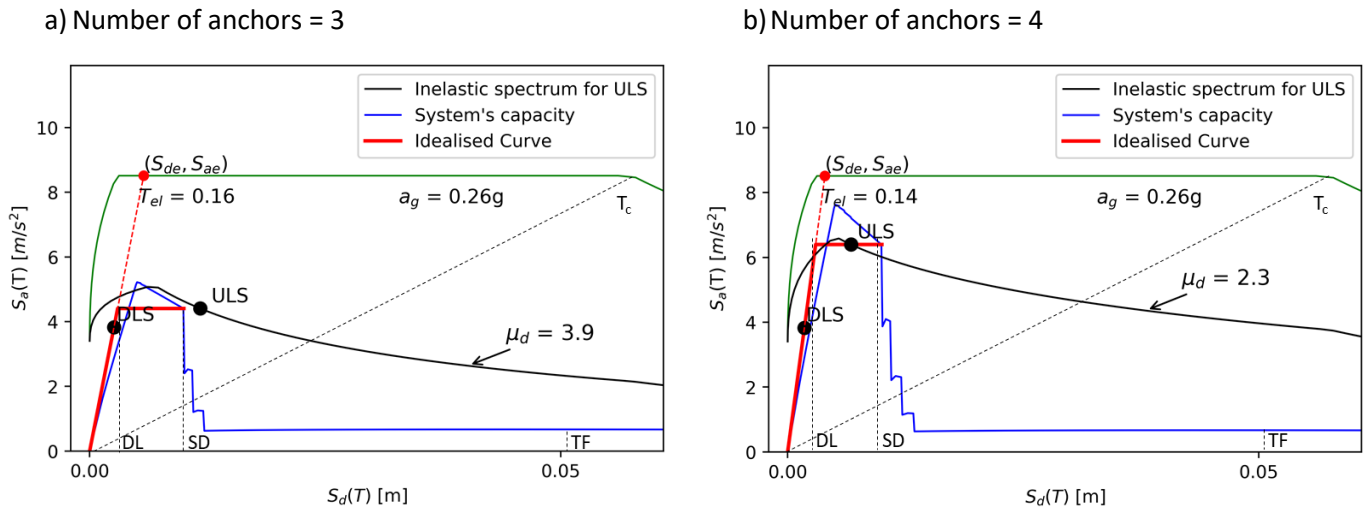


Fig. 14 Performance point determination for wall strengthened by three anchors a) and four anchors b).

### 4.3 Seismic performance of the structure strengthened by D-GAS

To further improve the response of the strengthened wall, the analysis is performed considering the D-GAS in place of traditional grouted anchors, meaning that Eq. (24) and Eq. (25) will determine the capacity curve and performance.

The performance points corresponding to the Damage and Ultimate limit states, shown in Fig. 15 , are both on the horizontal branch of the idealized system's capacity curve, meaning that the seismic demands will activate the device. The device determines an increment in the displacement capacity, with a "rigid shifting" of the critical points corresponding to "yielding" and "ultimate" displacement by a quantity equal to the device's displacement capacity. As a result, at the ULS limit state the device exploits half of its full sliding capacity. Moreover, the increased ductility determines a smaller acceleration demand which can be controlled by two anchors rather than four, thus reducing the impact on the aesthetic of the building, the installation costs, and the loss of original material.

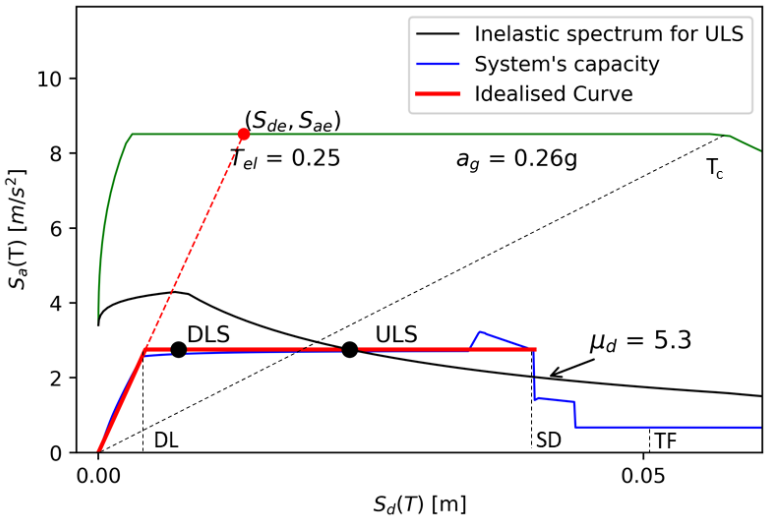


Fig. 15 Capacity curve and design check for wall strengthened by a dissipative device connected grouted anchors (D-GAS).

In conclusion, the use of the D-GAS has the main advantage of determining a smaller number of anchors. This is simply explained considering that a smaller number of anchors determines a smaller value of yielding acceleration $S_{ay}$ and reduces the initial stiffness of the system resulting into a larger elastic period and ductility demand $\mu_d$. Therefore, it is obtained that the inelastic demand is smaller in terms of accelerations and, from Eq. (16) and (32), larger in terms of displacement. A summary of the analyses' results performed for the different configurations is given in Table 6. The performance points for the DLS and ULS are compared to the DL and SD thresholds for each system, highlighting that the D-GAS provides the best design solution, as the implementation of the dissipative devices reduces the number of required anchors by 50%. For sake of comparison, the values stiffness of each system normalized to the stiffness of the wall in the unstrengthened configuration are reported in Table 6, as well as the ductility capacities.

Table 6 Summary of displacement demands and capacities for the wall in different configurations

| Configuration | Displacement capacity $\Delta_y$ [m] | Displacement capacity $\Delta_u$ [m] | Displacement demand DLS $\Delta_{DLS}$ [m] | Displacement demand ULS $\Delta_{ULS}$ [m] | Normalized Elastic stiffness [-] | Ductility capacity $\mu_c$ [-] | $\Delta_y > \Delta_{DLS}$ | $\Delta_u > \Delta_{ULS}$ |
|---|---|---|---|---|---|---|---|---|
| Original | 0.007 | 0.05 | 0.03 | 0.07 - 0.19 | 1 | 7.4 | NO | NO |
| 3 GAS | 0.003 | 0.01 | 0.002 | 0.013 | 15.1 | 3.3 | YES | NO |
| 4 GAS | 0.003 | 0.01 | 0.002 | 0.008 | 21.95 | 3.3 | YES | YES |
| 2 D-GAS | 0.004 | 0.04 | 0.008 | 0.026 | 6.5 | 9.3 | Yes-Sliding | Yes-Sliding |

### 4.4 . Seismic performance of the original structure – Dynamic analysis

The resulting rocking motions of the unstrengthened wall for the DLS and ULS are reported in Fig. 16, along with the accelerations at the Control Point (CP) and the damage thresholds. For the seismic acceleration scaled to the DLS the maximum displacement of the control point exceeds the DL limit $\Delta_y$, namely the displacement corresponding to the beginning of the plastic phase on the idealized curve. Similarly, for the ULS, a maximum displacement of 12 cm is reached at about 2 seconds, well above the displacement of the SD threshold $\Delta_{TC}$, reported in Fig. 16b as a red dotted line. Nonetheless, the wall survives the ground motion and the OOP failure: the rotations are about 12% the ultimate rotation $\alpha$ that the wall can withstand.

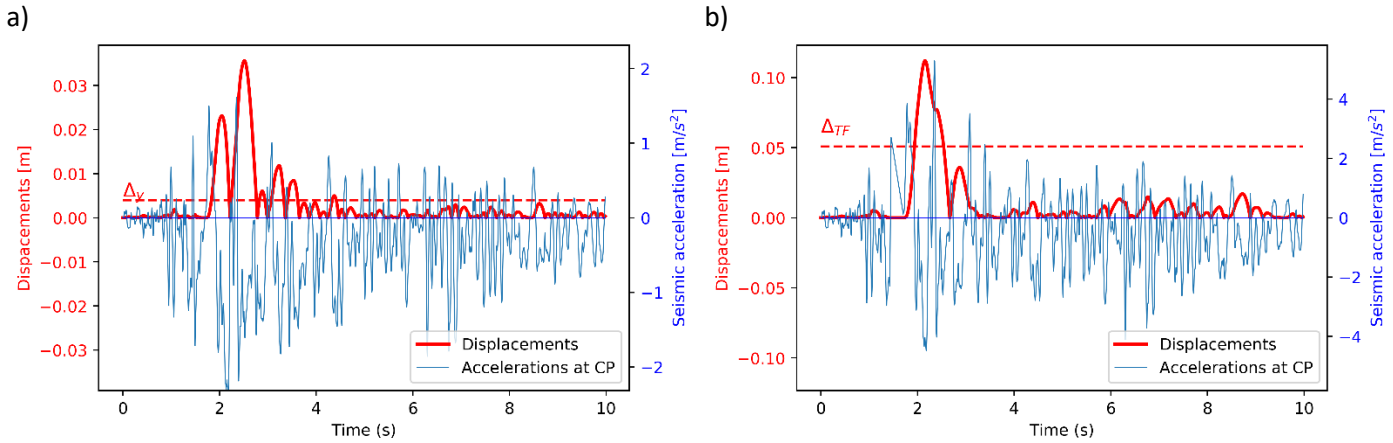


Fig. 16 Rocking motion of unstrengthened wall: displacements of control point and seismic input a) at Damage b) at Ultimate limit state

These results are in line with what obtained by the DB approach, which predicted that the displacement demands would exceed the damage thresholds for both limit states. Nonetheless, the maximum displacement at ULS ($\Delta_{max,rk} = 0.12m$) is 70% larger than the corresponding displacement predicted by static analysis ($\Delta_{ULS} = 0.07m$) as it is recognised that the period of vibration of rocking walls depends on the oscillation's amplitude [4,52]. Therefore, for large magnitude of OOP displacement computed using conventional elastic-based capacity curve, the oscillation's amplitude could be highly underestimated and the most accurate way to assess wall displacements and ultimately wall failure condition is to compute the wall response by integrating the equations of motion.

Conversely, good agreement between static and dynamic demand is obtained for the DL limit state where the vibrations have smaller amplitudes: the dynamic response confirms that the maximum base rotation is below the rotation limit for the toe-crushing failure and the maximum displacement of the control point is close to the one predicted by the DB approach.

A second dynamic analysis is performed for the wall strengthened by traditional grouted anchors and the dissipative anchoring system to check the design solutions proposed in the previous sections. Moreover, the analysis aims at evaluating the dissipative capacity of the D-GAS compared to a traditional anchoring system.

### 4.5 Analysis results – the strengthened configuration

The direct integration of the equation of motion is performed for a model of rocking wall including the strengthening systems. For the GAS, Eq. (30) is solved considering the design obtained following the FB and DB approaches to check if the number of anchors is sufficient to prevent the wall from experiencing large rocking oscillations. The rocking motion displayed in Fig. 17a shows that the anchoring system fails if 3 anchors are placed on each side of the façade: the anchors reach their full load and displacement capacity at about 2 seconds when the horizontal displacement of the CP is equal to 1 cm. It is assumed that the wall behaves as if unstrengthened after the anchor's failure (point "AF" in Fig. 17a) even if they would keep providing a restraining action on the façade in a real scenario. Nonetheless this action would be limited as highlighted by pull-out tests where the anchor's force reduces up to 70% for large slippage [10,11] and it is safely assumed equal to zero.

With reference to the case of an unstrengthen wall, it is evident that the GAS determines a change in the wall's response, delaying the peak oscillation's amplitude. Nonetheless, after the anchors have failed, large horizontal displacements that would cause severe damages and cracks to the structure are computed.

The analysis confirms that the dimensioning of the GAS provided by the force-based design is not adequate. As the system has limited ductility, the value of behaviour factor q =2.0 suggested by the code to compute the horizontal acceleration multiplier should be reduced, as there is no guaranty that once the motion is activated the ultimate displacement is not exceeded. The value of q = 1.0 suggested by [4] for rocking systems with limited displacement capacity should be used in Eq. (34) instead to determine the correct number of anchors.

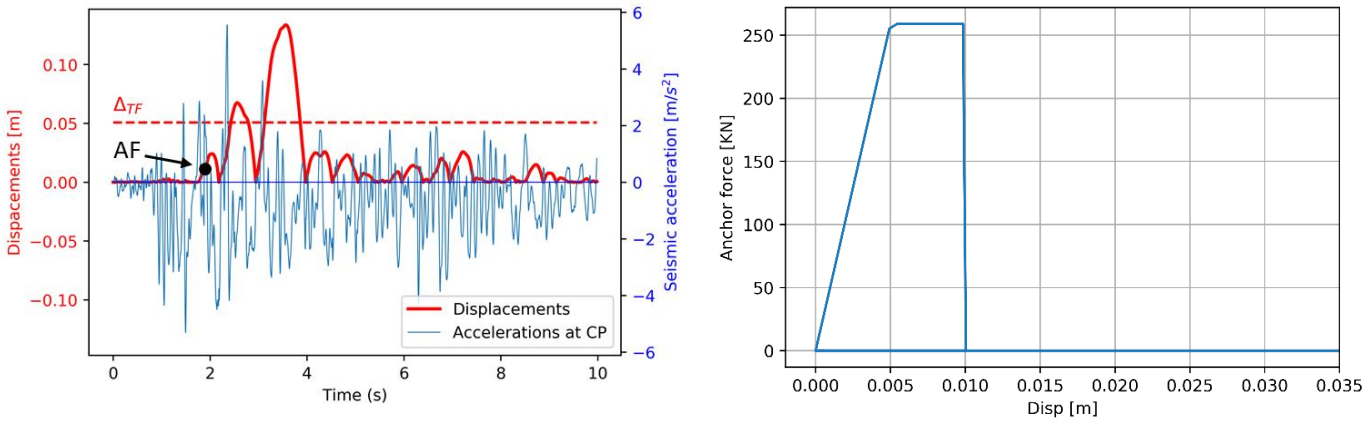


Fig. 17 Rocking motion of wall strengthened by GAS: a) displacements of control point and seismic input, b) load-displacement loops of anchoring system if three anchors are provided.

A third dynamic analysis is conducted considering the number of anchors (n = 4) suggested by the DB approach with the resulting displacement history shown in Fig. 18a. As shown in Fig. 18b, the GAS yields, but it does not fail for the whole duration of the seismic action, as predicted by the static method.

The anchors undergo a large number of oscillations with small amplitude due to the high stiffness of the system. Despite the large number of oscillations, the amplitude of the rotations is below the anchor's yielding threshold ( $\Delta_y$ in Fig. 18a) in more than 50% of the cases, resulting in a small value of dissipated energy, as reported in Table 7.

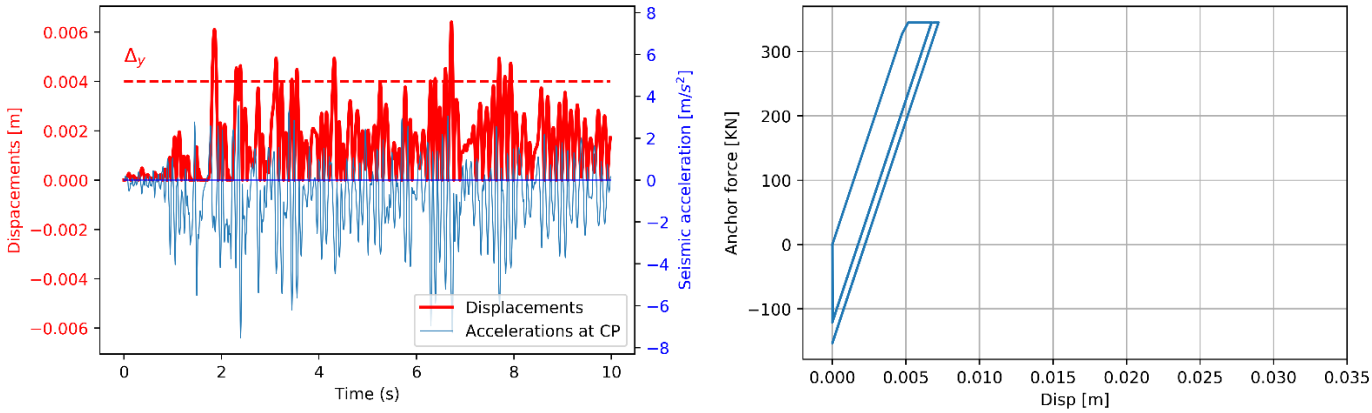


Fig. 18 Rocking motion of wall strengthened by GAS: a) displacements of control point and seismic input, b) load-displacement loops of anchoring system if four anchors are provided.

Finally, the analysis is performed for the case of wall strengthened by the D-GAS. According to the DB design, two anchors equipped with the dissipative device are considered on each side to connect the façade to the side walls. The device is set to start sliding at 80% of the maximum capacity of the single anchor ($C_{DAS} = 0.8$). According to the displacement limit indicated by Eq. (26) the allowable run of the device is set at 30 mm, which corresponds to an improvement in displacement capacity with respect to the GAS of $\eta = 4$. The rocking motion and dissipative loops are reported in Fig. 19. The maximum amplitude of the rocking motion is about 29mm (Fig. 19a), which well agrees with the displacement capacity identified by the performance point for the ULS. The device provides additional displacement capacity to the anchoring system, which slides without failing for the whole duration of the seismic event. This results in a large dissipation capacity: the area enclosed within the hysteresis curve shown in Fig. 19b represents the energy dissipated by the anchor for the duration of the seismic input and corresponds to 50% of the energy imparted to the system by the seismic input. Also, the friction device of the D-GAS works as a "braking system" providing an acceleration which is always opposite in direction to the seismic one, thus reducing by 36% the maximum acceleration that the system experiences compared to the unstrengthen wall.

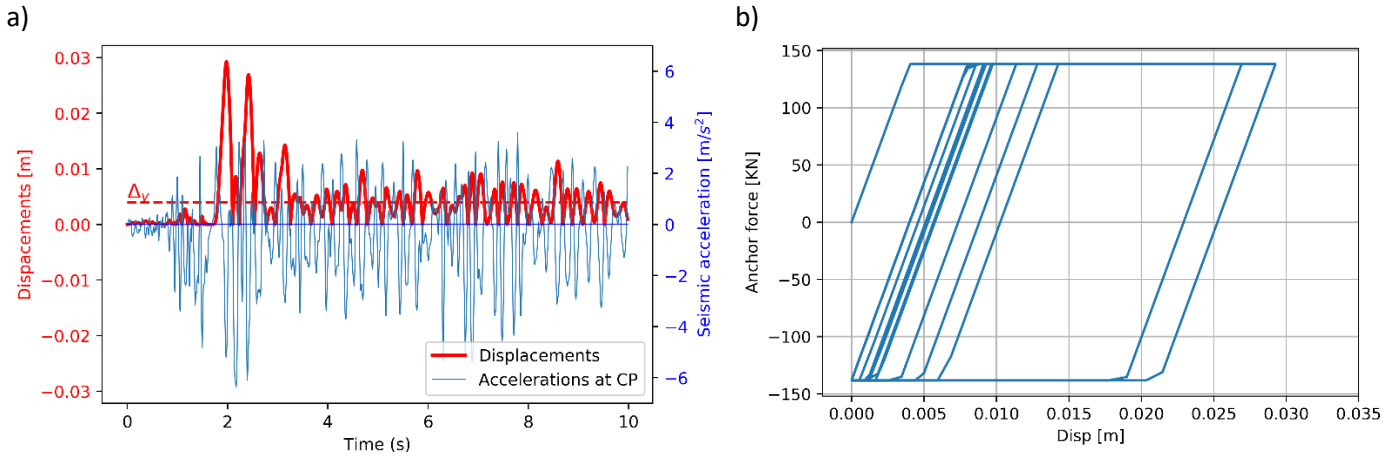


Fig. 19 Rocking motion of wall strengthened by D-GAS: a) displacements of control point and seismic input, b) Dissipative loops of two anchors.

Table 7 summarise the results of the dynamic analysis for the three configurations and the two limit states, showing the difference in dissipated energy registered by considering the use of the dissipative device by means of the ratio $\gamma$ defined by Eq. (33).

Table 7 Summary of time-history analysis performed for the wall in different configurations

| Configuration | η | Seismic Energy | | Dissipated Energy | | γ | | Max acceleration | | Max displacement | | β | |
|---|---|---|---|---|---|---|---|---|---|---|---|---|---|
| | [-] | $E_I$ [Kg m²/s²] | | $E_{D\ (GAS/DAS)}$ [Kg m²/s²] | | [-] | | $a_{max}$ [m²/s²] | | $\Delta_{max,rk}$ [m] | | [-] | |
| | | DLS | ULS | DLS | ULS | DLS | ULS | DLS | ULS | DLS | ULS | DLS | ULS |
| Original | - | 1207 | 3582 | 0 | 0 | 0% | 0% | 1.61 | 5.57 | 0.035 | 0.12 | 0.86 | 0.6 |
| 3 GAS | 1 | 538 | 5576 | 0 | 194 | 0% | 3% | 1.41 | 5.55 | 0.002 | 0.13 | 1.00 | 0.10 |
| 4 GAS | 1 | 524 | 3291 | 0 | 48 | 0% | 1% | 1.68 | 3.56 | 0.002 | 0.007 | 1.00 | 1.14 |
| 2 DAS ($C_{DAS}$ = 0.8) | 4 | 611 | 3533 | 7.6 | 1776 | 1% | 50% | 1.41 | 3.54 | 0.005 | 0.029 | 1.60 | 0.90 |

At DLS the amount of energy dissipated by the anchorage with and without the device is negligible, between 0 and 1% of the input energy. This is simply explained considering that the anchor remains in its elastic phase and that the seismic load is sufficient to induces just few millimetres of slippage in the devices. Good agreement is found between the seismic displacement demand and the maximum displacement obtained by rocking analysis, with values of $\beta$ close to 1 in most of the cases. The worst result was obtained for the ULS and 3 anchors as obtained from the FB design: as pointed out before, this anchoring design is not sufficient to resist the displacement demand and would lead to the failure of the system after which large displacement are obtained. This means that the $\mu - T$ relation presented in Eq. (17) provides a good approximation of the ductility and energy dissipation of the system and therefore can be adopted also for the case of rocking walls strengthened by traditional and innovative anchors.

Both the GAS with four anchors and the D-GAS with two anchors provide effective strengthening solutions, but it is clear that the D-GAS represents the optimal design in term of reduced accelerations, energy dissipated, and minimal disruption to the system's integrity.

## 5 Conclusions

Historic masonry buildings are severely affected by seismic events and often experiencing out-of-plane (OOP) failure due to the poor quality of connections between orthogonal walls. Design codes stress the importance of providing effective connections during the seismic upgrade of heritages structures, so as to achieve a more favourable

redistribution of inertial loads, but the prescriptions are mainly qualitative. To address this issue, this study presents a displacement-based (DB) design procedure for seismic upgrade of historic masonry buildings by means of grouted anchoring systems (GAS).

This anchor typology can be preferred to steel ties as it does not require anchor plates to transfer the load from the rebar to the parent material, thus minimizing the impact of the installation on the aesthetic of the building. The design of anchorages is typically performed according to a Force-based design, ensuring that the load capacity of the anchors is greater than the seismic demand. The latter is computed as the mass of the wall's portion assigned to each anchor times the seismic acceleration; the load capacity of the anchors is determined analytically and then by in-situ and experimental pull-out test to verify the effective bonding capacity that the anchor develops with the masonry.

Nonetheless, a review of the pull-out tests performed on grouted anchors have highlighted that they present limited displacement capacity which determines load degradation under cyclic loading soon after the maximum load capacity is reached. This can hamper the use of grouted anchors as aseismic system: according to the EN 15129 provisions, the reduction in load capacity should not excel 10% under cyclic loading.

To tackle this issue a Dissipative Grouted Anchoring System (D-GAS) has been developed, connecting a friction-based dissipative device to the tie rods of the GAS. When the load induced by a seismic event exceeds the slippage load of the device, the wall starts rocking in its OOP direction up to a maximum amplitude of oscillations which is determined by the displacement capacity of the device itself. Along with the energy lost at each impact of the wall with the base and side wall, the device provides a second source of energy dissipation, reducing the stress distribution at the interface between the anchor and the parent material. Ultimately, this results in less damage to the structure and to the anchoring system.

The design method presented in this study identifies a set of threshold values that the wall strengthened by either the GAS or the D-GAS should not exceed to preserve its integrity during its rocking motion. For the GAS the limits are obtained by reviewing seven studies on experimental pull-out test and normalizing the recorded displacements to the value of embedment length. The obtained longitudinal slip strain at which the loss in load capacity is equal to 20% is taken as ultimate strain value. For the D-GAS, the ultimate strain is increases by a quantity directly proportional to the device's displacement capacity, which shall not exceed the displacement corresponding to the toe-crushing failure. Then, the design procedure is performed computing the performance points for the system with respect to a seismic action and verifying that the displacement demands are smaller than the threshold values. Finally, to verify the design procedure and quantify the benefit of adding the dissipative device to grouted anchors, the design solutions proposed for the GAS and D-GAS are compared looking at the dynamic evolution of the wall in each configuration (unstrengthened wall, wall with GAS, wall with D-GAS) obtained performing a time-history analysis. Some key assumptions are made in developing the model, such as a vertical crack at the wall's intersection and considering the portion of anchor grouted in the side wall as fixed. This assumptions are based on past experimental tests' results [26] and on an experimental activity currently ongoing by the authors, which will be available in future journal publications.

The method is applied to the façade of the oratory of San Giuseppe dei Minimi, which rocked without collapsing during the L'Aquila (IT) 2009 earthquake to compare the performance of the historic building in its original configuration, and as restrained by grouted anchoring system with and without the device inclusion.

The results show that the unstrengthened façade would display large displacements under the considered seismic action causing large crack openings at the corner connection. The implementation of the GAS significantly increases the connection's stiffness and prevents the crack opening. Given the limited displacement capacity that the anchor display, the design of the GAS should be performed according to a DB design, which verifies that the displacement demand is smaller than the anchor's capacity. Conversely, a design procedure based on a force-only procedure led to an inadequate design for the presented case-study as the number of anchors was insufficient to resist the displacement demand. This is explained considering that typical Force-based design procedures refer to dry anchors which are designed to plastically yield and display a larger displacement capacity compared to their grouted counterpart. Therefore, the value of behaviour factor, $q = 2$, assumed for the FB design of dry anchors should be reduced to $q = 1$ for the case of grouted anchors.

The building performance increases if the D-GAS is considered as larger ductility capacity allows for a reduction in the seismic demand and thus a smaller number of anchors is required to resist the horizontal loading. The wall displays a controlled rocking motion, with the oscillation's amplitude below the threshold value identifying the toe-crush failure. The D-GAS activates without causing the anchor's debonding both for the Ultimate Limit State and the Damage Limit State, proving that the system is beneficial also for less intense earthquakes as it is able to damp the seismic accelerations that could cause damages to the artic assets of the building. At ULS the D-GAS dissipates 50% of the seismic energy, compared to just 1% of traditional grouted anchors, and reduces the linear accelerations at the control point by 37% with respect to the wall in its original configuration.

These results highlight that the dissipative device is fit for the seismic strengthening of masonry structures. In particular, historic buildings would benefit of the implementation of the innovative system connected to grouted anchors because it would reduce the number of the required anchors, resulting in less invasive installation procedures.

The comparison with the results of the dynamic analysis, shows that the design procedure is able to provide a reliable method for determining the vulnerability of walls to OOP failure and the optimal strengthening solution to control such motion and prevent severe damages to the structure. The proposed design procedure has a general value, as it could be extended to other anchoring system able to restrain the OOP motion. For instance, the procedure can be easily adapted to steel ties connecting opposite walls, by defining the constitutive law correlating the yielding elongation of the ties to the base rotation of the wall.

**Funding declaration**

This research was supported jointly by Cintec International and UCL through a UCL Industry Impact studentship.

**Declaration of Competing Interest**

The authors declare that they have no known competing financial interests or personal relationships that could have appeared to influence the work reported in this paper.

**Acknowledgments**

The authors wish to acknowledge the long-lasting partnership with Cintec International, which provided continuous technical and economic support.

# 6 References

[1] D. D'Ayala, S. Paganoni, Assessment and analysis of damage in L'Aquila historic city centre after 6th April 2009, Bull. Earthq. Eng. 9 (2011) 81–104. https://doi.org/10.1007/s10518-010-9224-4.

[2] L. Moon, D. Dizhur, I. Senaldi, H. Derakhshan, M. Griffith, G. Magenes, J. Ingham, The demise of the URM building stock in Christchurch during the 2010-2011 Canterbury earthquake sequence, Earthq. Spectra. 30 (2014) 253–276. https://doi.org/10.1193/022113EQS044M.

[3] V. Putrino, D. D'Ayala, Effectiveness of seismic strengthening to repeated earthquakes in historic urban contexts: Norcia 2016, Disaster Prev. Manag. An Int. J. 29 (2019) 47–64. https://doi.org/10.1108/DPM-07-2018-0230.

[4] L. Sorrentino, D. D'Ayala, G. de Felice, M.C. Griffith, S. Lagomarsino, G. Magenes, Review of Out-of-Plane Seismic Assessment Techniques Applied To Existing Masonry Buildings, Int. J. Archit. Herit. 11 (2017) 2–21. https://doi.org/10.1080/15583058.2016.1237586.

[5] V. Doglioni, F., Moretti, A. & Petrini, Le chiese e il terremoto, Edizioni L, Trieste, 1994.

[6] D. D'Ayala, E. Speranza, Definition of Collapse Mechanisms and Seismic Vulnerability of Historic Masonry Buildings, Earthq. Spectra. 19 (2003) 479–509. https://doi.org/10.1193/1.1599896.

[7] S. Lagomarsino, S. Podestà, S. Resemini, E. Curti, S. Parodi, Mechanical modets for the seismic vulnerability assessment of churches, 4th Int. Semin. Struct. Anal. Hist. Constr. (2004) 1091–1101. http://www.hms.civil.uminho.pt/sahc/2004/1091.pdf.

[8] B. Gigla, F. Wenzel, Design recommendations for injection anchors as supplementary reinforcement of historic masonry, 12th Int. Brick/Block Mason. Conf. (2000) 691–706.

[9] F. Arifovic, M.P. Neilsen, Strength of Anchors in Masonry, 2006.

[10] S. Paganoni, D. D'Ayala, Testing and design procedure for corner connections of masonry heritage buildings strengthened by metallic grouted anchors, Eng. Struct. 70 (2014) 278–293. https://doi.org/10.1016/j.engstruct.2014.03.014.

[11] S. Moreira, L.F. Ramos, D. V. Oliveira, P.B. Lourenço, Experimental behavior of masonry wall-to-timber elements connections strengthened with injection anchors, Eng. Struct. 81 (2014) 98–109. https://doi.org/10.1016/j.engstruct.2014.09.034.

[12] F. Silveri, P. Riva, G. Profeta, E. Poverello, C. Algeri, Experimental Study on Injected Anchors for the Seismic Retrofit of Historical Masonry Buildings, Int. J. Archit. Herit. 10 (2016) 182–203. https://doi.org/10.1080/15583058.2015.1113333.

[13] F. Ceroni, R. Cuzzilla, M. Pecce, Assessment of performance of steel and GFRP bars as injected anchors in masonry walls, Constr. Build. Mater. 123 (2016) 78–98. https://doi.org/10.1016/j.conbuildmat.2016.06.124.

[14] F. Ceroni, M. Di Ludovico, Traditional and innovative systems for injected anchors in masonry elements : Experimental behavior and theoretical formulations, Constr. Build. Mater. 254 (2020) 119178. https://doi.org/10.1016/j.conbuildmat.2020.119178.

[15] CMIT, Ministero delle Infrastrutture e dei trasporti. Circolare 2 febbraio 2009 , n. 617, Contenente Le Istruzioni per L'applicazione Delle "Nuove Norme Tecniche per Le Costruzioni" Di Cui Al DM 14 Gennaio 2008. Gazzetta Ufficiale della Repubblica Italiana n. 4, 2009.

[16] EN 1998-1:2004, Design of structures for earthquake resistance, London, 2004.

[17] O. AlShawa, D. Liberatore, L. Sorrentino, Dynamic One-Sided Out-Of-Plane Behavior of Unreinforced-Masonry Wall Restrained by Elasto-Plastic Tie-Rods, Int. J. Archit. Herit. 13 (2019) 340–357. https://doi.org/10.1080/15583058.2018.1563226.

[18] K. Doherty, M.C. Griffith, N. Lam, J. Wilson, Displacement-based seismic analysis for out-of-plane bending of unreinforced masonry walls, Earthq. Eng. Struct. Dyn. 31 (2002) 833–850. https://doi.org/10.1002/eqe.126.

[19] O. Al Shawa, G. Felice, A. Mauro, L. Sorrentino, Out-of-plane seismic behaviour of rocking masonry walls, Earthq. Eng. Struct. Dyn. 41 (2012) 949–968. https://doi.org/10.1002/eqe.1168.

[20] D. D'Ayala, Y. Shi, Modeling masonry historic buildings by multi-body dynamics, Int. J. Archit. Herit. 5 (2011) 483–512. https://doi.org/10.1080/15583058.2011.557138.

[21] S. Giovinazzi, S. Lagomarsino, S. Resemini, Displacement capacity of ancient structures through non-linear kinematic and dynamic analyses, Struct. Anal. Hist. Constr. (2006) 1–10. http://ir.canterbury.ac.nz/handle/10092/4127.

[22] D.F. D'ayala, Force and displacement based vulnerability assessment for traditional buildings, Bull. Earthq. Eng. 3 (2005) 235–265. https://doi.org/10.1007/s10518-005-1239-x.

[23] D. D'Ayala, S. Paganoni, Testing and design protocol of dissipative devices for out-of-plane damage, Proc. Inst. Civ. Eng. Struct. Build. 167 (2014) 26–40. https://doi.org/10.1680/stbu.12.00087.

[24] V. Melatti, D. D'Ayala, Methodology for the assessment and refinement of friction-based dissipative devices, Eng. Struct. 229 (2020) 111666. https://doi.org/10.1016/j.engstruct.2020.111666.

[25] E. Giuriani, A. Marini, Experiences from the Northern Italy 2004 earthquake: Vulnerability assessment and strengthening of historic churches, Struct. Anal. Hist. Constr. Preserv. Saf. Significance - Proc. 6th Int. Conf. Struct. Anal. Hist. Constr. SAHC08. 1 (2008) 13–24.

[26] S. Paganoni, Dissipative Anchor Devices for the Seismic Retrofit of Heritage Buildings, Ph.D. Thesis, Univ. Bath, Dep. Archit. Civ. Eng. 1 (2015).

[27] EN 1881:2006, Products and systems for the protection and repair of concrete structures – test methods – testing of anchoring products by pull-out method, 2006.

[28] EN 846-2:2000, Methods of test for ancillary components for masonry. Part 2: determination of bond strength of prefabricated bed joint reinforcement in mortar joints, (2000).

[29] C. Algeri, E. Poverello, G. Plizzari, E. Giuriani, Experimental study on the injected anchors behaviour on historical masonry, Adv. Mater. Res. 133–134 (2010) 423–428. https://doi.org/10.4028/www.scientific.net/AMR.133-134.423.

[30] NIKER, Guidelines for assessment and improvement of connections in buildings, Final Reports D10.2 – New integrated knowledge based approaches to the protection of cultural heritage from earthquake induced risk, NIKER, Contract FP7-ENV-2009-1, n. 244123, 2012.

[31] B. Gigla, Bond Strength of Injection Anchors as Supplementary Reinforcement Inside Historic Masonry, in: 13th Int. Brick Block Conf., 2004: pp. 119–128.

[32] B. Gigla, Structural design of supplementary injection anchors inside masory, in: 15th Int. Brick Block Mason. Conf., 2012.

[33] R. Eligehausen, E.P. Popov, V. V. Bertero, Local Bond Stress-Slip Relationships of Deformed Bars Under Generalized Excitations., 4 (1982) 69–80.

[34] CEB, CEB, Comité Euro-International du Béton, Fastenings to concrete and masonry structures. State-of-the-art report, Thomas Telford, London, 1994.

[35] R. Park, Evaluation of ductility of structures and structural assemblages from laboratory testing, 22 (1989) 155–166.

[36] G. Maddaloni, M. Di Ludovico, A. Balsamo, A. Prota, Out-of-plane experimental behaviour of T-shaped full scale masonry wall strengthened with composite connections, Compos. Part B Eng. 93 (2016) 328–343. https://doi.org/10.1016/j.compositesb.2016.03.026.

[37] G.T. Doerr, R.E. Klingner, Adhesive anchors: behaviour and spacing requirements, Res. Rep. No. 1126-2. (1989).

[38] D.F. D'Ayala, M. Forsyth, What is Conservation Engineering?, Struct. Constr. Hist. Build. Conserv. (2008) 1–11. https://doi.org/10.1002/9780470691816.ch1.

[39] R.A. Cook, Behaviour of chemically bonded anchors., J. Struct. Eng. 119(9):274 (1993).

[40] M.S.J.C. MSJC, Building Code Requirements for Masonry Structures, (TMS 402-13/ACI, 530-13/ASCE), 2013.

[41] A.S. Araújo, D. V. Oliveira, P.B. Lourenço, Numerical study on the performance of improved masonry-to-timber connections in traditional masonry buildings, Eng. Struct. 80 (2014) 501–513. https://doi.org/10.1016/j.engstruct.2014.09.027.

[42] L. Giresini, M.L. Puppio, F. Taddei, Experimental pull-out tests and design indications for strength anchors installed in masonry walls, Mater. Struct. Constr. 53 (2020) 1–16. https://doi.org/10.1617/s11527-020-01536-2.

[43] EN 15129, CEN/TC 340 Anti-seismic devices, 2006.

[44] D. D'Ayala, Assessing the seismic vulnerability of masonry buildings, 2013. https://doi.org/10.1533/9780857098986.3.334.

[45] S. Lagomarsino, Seismic assessment of rocking masonry structures, Bull. Earthq. Eng. 13 (2015) 97–128. https://doi.org/10.1007/s10518-014-9609-x.

[46] P. Fajfar, A Nonlinear Analysis Method for Performance-Based Seismic Design, Earthq. Spectra. 16 (2000) 573–592. https://doi.org/10.1193/1.1586128.

[47] A.A. Costa, A. Arêde, A. Penna, A. Costa, Free rocking response of a regular stone masonry wall with equivalent block approach: experimental and analytical evaluation, Pacific Conf. Earthq. Eng. (2013) 1–6. https://doi.org/10.1002/eqe.2327.

[48] A. Mehrotra, M.J. DeJong, The influence of interface geometry, stiffness, and crushing on the dynamic response of masonry collapse mechanisms, Earthq. Eng. Struct. Dyn. 47 (2018) 2661–2681. https://doi.org/10.1002/eqe.3103.

[49] O. AlShawa, L. Liberatore, D. Liberatore, F. Mollaioli, L. Sorrentino, Seismic Demand on a Unreinforced Masonry Wall Restrained by Elasto-Plastic Tie-Rods Under Earthquake Sequences, Int. J. Archit. Herit. 13 (2019) 1124–1141. https://doi.org/10.1080/15583058.2019.1645239.

[50] M. Dolšek, P. Fajfar, The effect of masonry infills on the seismic response of a four-storey reinforced concrete frame - a deterministic assessment, Eng. Struct. 30 (2008) 1991–2001. https://doi.org/10.1016/j.engstruct.2008.01.001.

[51] D.P. Abrams, O. AlShawa, P.B. Lourenço, L. Sorrentino, Out-of-Plane Seismic Response of Unreinforced Masonry Walls: Conceptual Discussion, Research Needs, and Modeling Issues, Int. J. Archit. Herit. 11 (2017) 22–30. https://doi.org/10.1080/15583058.2016.1238977.

[52] G. Housner, The behaviour of inverted pendulum structures during earthquakes, 53 (1963) 403–417.

[53] L. Sorrentino, O. AlShawa, L.D. Decanini, The relevance of energy damping in unreinforced masonry rocking mechanisms. Experimental and analytic investigations, Bull. Earthq. Eng. 9 (2011) 1617–1642. https://doi.org/10.1007/s10518-011-9291-1.

[54] F. Ferreira, C. Moutinho, Á. Cunha, E. Caetano, An artificial accelerogram generator code written in Matlab, Eng. Reports. 2 (2020) 1–17. https://doi.org/10.1002/eng2.12129.

[55] O. Al Shawa, Dinamica non lineare fuori piano di pareti murarie. Stato dell'arte, sperimentazione e modellazione, Roma, Sapienza, 2011.

[56] ICOMOS, Icomos Charter- Principles for the Analysis , Conservation and Structural Restoration of Architectural Heritage (2003), 2003.